

RESEARCH ARTICLE

Open Access



# Defining multiple inhabitations of a cave environment using interdisciplinary archaeometry: the 'Christmas Cave' of the Wadi en-Nar/Nahal Qidron, West of the Dead Sea

Kaare Lund Rasmussen<sup>1\*</sup> , Johannes van der Plicht<sup>2</sup>, Ilaria Degano<sup>3</sup>, Francesca Modugno<sup>3</sup>, Maria Perla Colombini<sup>3</sup>, Guillermo de la Fuente<sup>4</sup>, Thomas Delbey<sup>5</sup>, Amos Frumkin<sup>6</sup>, Uri Davidovich<sup>7</sup>, Roi Porat<sup>7</sup>, Orit Shamir<sup>8</sup>, Naama Sukenik<sup>8</sup>, Greg Doudna<sup>9</sup>, Joan Taylor<sup>10</sup> and Mladen Popović<sup>11</sup>

## Abstract

The present study reports a series of interdisciplinary archaeometrical analyses of objects found in the Christmas Cave, which was discovered by John Allegro and his team in 1960 on the West Bank of the Dead Sea and assumed to be inhabited only in the Chalcolithic era and by Jewish refugees of the second century CE, at the end of the Bar Kokhba Revolt. Like many other Judaeen desert caves, there was an abundance of organic material, especially textiles, surviving in the dry environment. In the absence of clear stratigraphy and even a proper publication of the finds, the present study shows how archaeometry can provide important insights. We analysed food crusts on ceramics by gas chromatography with mass spectrometric detection (GC–MS), made petrographic descriptions to estimated provenance of the ceramics, produced new radiocarbon dates from organic material and thermoluminescence (TL) dates from the pottery. It appears from the data that the Christmas Cave has been briefly inhabited or visited intermittently over a very long time, starting ca. 4000 BCE (the Chalcolithic period), and extending all the way to the Medieval period, even though there is also a concentration of dates near the period of the Bar Kokhba Revolt (132–136 CE). We argue, through a detailed analysis of the radiometric and TL-datings and by the artefactual evidence, that there was likely another refuge episode connected with the First Jewish Revolt during which people fled to this cave. However, we see no material connection to Qumran and nearby caves. Overall, our study demonstrates the importance of archaeometric studies in cave environments where stratigraphy is veritably absent.

**Keywords:** Christmas Cave, Judean Desert, Bar Kokhba Revolt, Radiocarbon dating, TL-dating, Ceramic analyses, Organic residue analyses, Textiles

## Introduction

Cave environments are often particularly challenging to archaeologists when it comes to the dating of artefacts found within them. Caves frequently lack significant stratigraphy, one of the cornerstones of defining

human occupation, though at times this can be built up by series of rockfalls, debris or even collections of animal droppings. Therefore, when artefacts that do not show clear typological features are found, what appears to be an assemblage from one period can actually come from multiple times, and attest to different events of human activity, and from long term use to sporadic visits. In recent work on Cave 11Q near Qumran, on the coast of the Dead Sea, a range of scientific methods were employed on artefacts alongside classic typological

\*Correspondence: klr@sdu.dk

<sup>1</sup> Institute of Physics, Chemistry and Pharmacy, University of Southern Denmark, Campusvej 55, 5230 Odense M, Denmark  
Full list of author information is available at the end of the article

analyses, revealing a far more complex picture of human inhabitation of the cave than had hitherto been assumed (see [1]). In the present study, we deploy a range of interdisciplinary studies in key fields of archaeometry. We consider another cave in the Judean wilderness, the so-called ‘Christmas Cave’, in order to probe whether use of these scientific methods can further nuance conclusions about human inhabitation of a cave environment, and the identity of the people who came here. As in other Judean Desert caves, the Christmas Cave is regarded as a ‘time capsule’ preserving various finds from several periods, but with little stratification, and little data from the cave has hitherto been published or studied.

### The Christmas Cave: location and excavation

The Christmas Cave was discovered by John Allegro and Howard Stutchbury on Christmas Day of 1960, when they were engaged in excavations at Khirbet Mazin (Fig. 1). After a small initial sounding, it was excavated over two seasons by the British Dead Sea Scrolls Foundation (DSSF), under licence from Jordan, in December 1961 to January 1962 and again in December 1962 to January 1963. While the team’s original hope was that this cave could yield more Dead Sea Scrolls, only tiny pieces of one papyrus written in Greek were found, and they never fully published either this or the other artefacts they excavated [2, 3].

The Christmas Cave is located in the eastern segment of Nahal Kidron/Qidron (Wadi an-Nar), near the top of the south-western bank of the wadi, before its last turn eastwards towards the lower canyon, at coordinates 239887/621095 (New Israel Grid), ca. 3 km west of the Dead Sea and 8 km SSW of Qumran. Allegro described the structure of the cave and also reported signs of looting conducted by Bedouins that preceded his visit ([2]: pages 11–13 [3]). Artefacts from the cave were in fact offered to the excavators in due course, and included wooden bowls, spindle whorls, a distaff, combs, kohl container and stick, a seal, beads, an ivory-inlaid box, coins, and an adze handle. The excavations proper brought to light numerous artefacts, amongst them textiles, wood, leather, basketry, metals, ceramics, glass, and flint. A bronze coin minted during the second year of the Bar Kokhba Revolt (132–136 CE), as well as Roman-period pottery, pieces of leather (some from shoes), small fragments of papyrus and a large number of textiles cumulatively corresponding with an interpretation of the cave as a primarily being a place of refuge in the Roman period, likely the second century. At this time, refugees fled to numerous caves of the Judean Desert after the revolt, led by Shimon ben Kosiba (called Bar Kokhba) was brutally quashed by Roman forces.

However, there was also a flint blade and a bone tool assigned to the Chalcolithic period, and the adze handle was also identified as Chalcolithic.

Part of the history of the discovery of the cave and of the excavations was briefly reported by Allegro in his popular book entitled *Search in the Desert* [2], though Allegro did not present the actual findings and excavations accurately, and only his archives provide the full story (see [3]; these are currently being prepared for publication).

The two seasons of excavations in the cave were never published, owing to political changes. The objects were placed in boxes in the Rockefeller Museum (Palestine Archaeological Museum) close to the storage area of Qumran. After the Six Day war of 1967, the British excavation teams did not further the publication, owing to their close association with the Jordanian royal family. As time passed, the exploration of the Christmas Cave did not attract scholarly attention, and even its location was forgotten due to the lack of geographic references in Allegro’s publication. In the 1980s, the stored boxes were opened by the École Biblique et Archéologique de Française (EBAF) and assumed to have come from an unidentified Qumran cave. At this point they were erroneously assigned the prefix QCC, short for ‘Qumran Christmas Cave’. When the study of the material culture of Qumran was resumed in the 1990’s, under the auspices of EBAF, the Christmas Cave was understood as one of the Qumran caves (e.g. [4]). It took some effort before the location of the Christmas Cave was re-traced again in 2007 by the Israel Cave Research Center of the Hebrew University of Jerusalem [5–7]. This renewed salvage investigation included a speleological and archaeological survey, and brought forward numerous finds, including potsherds, two additional bronze coins (and two more found in small alcoves next to the cave entrance), textile fragments, vegetal food remains, and metal objects.

In tandem, analyses conducted on the finds collected by Allegro began to indicate that the cave experienced human presence in multiple periods, including the Late Chalcolithic, Early Bronze Age I, Early Roman (first century CE), as well as during the Bar Kokhba Revolt [4, 6, 8–12]. Especially telling were the detailed studies devoted to the large collection of textiles [4, 10, 11, 13, 14]. Of the 255 catalogued textiles, 71 linen textiles were attributed to the Chalcolithic period; five pieces were assigned to the Medieval era, together with several modern textiles made of cotton; and the remaining 184 textiles were assigned to the Roman period. The textiles from the Roman period included 113 made of wool, 63 of linen, and 8 of goat-hair [11, 14]. Some of the Roman wool textiles were dyed or decorated with bands or a gamma-shaped design using a

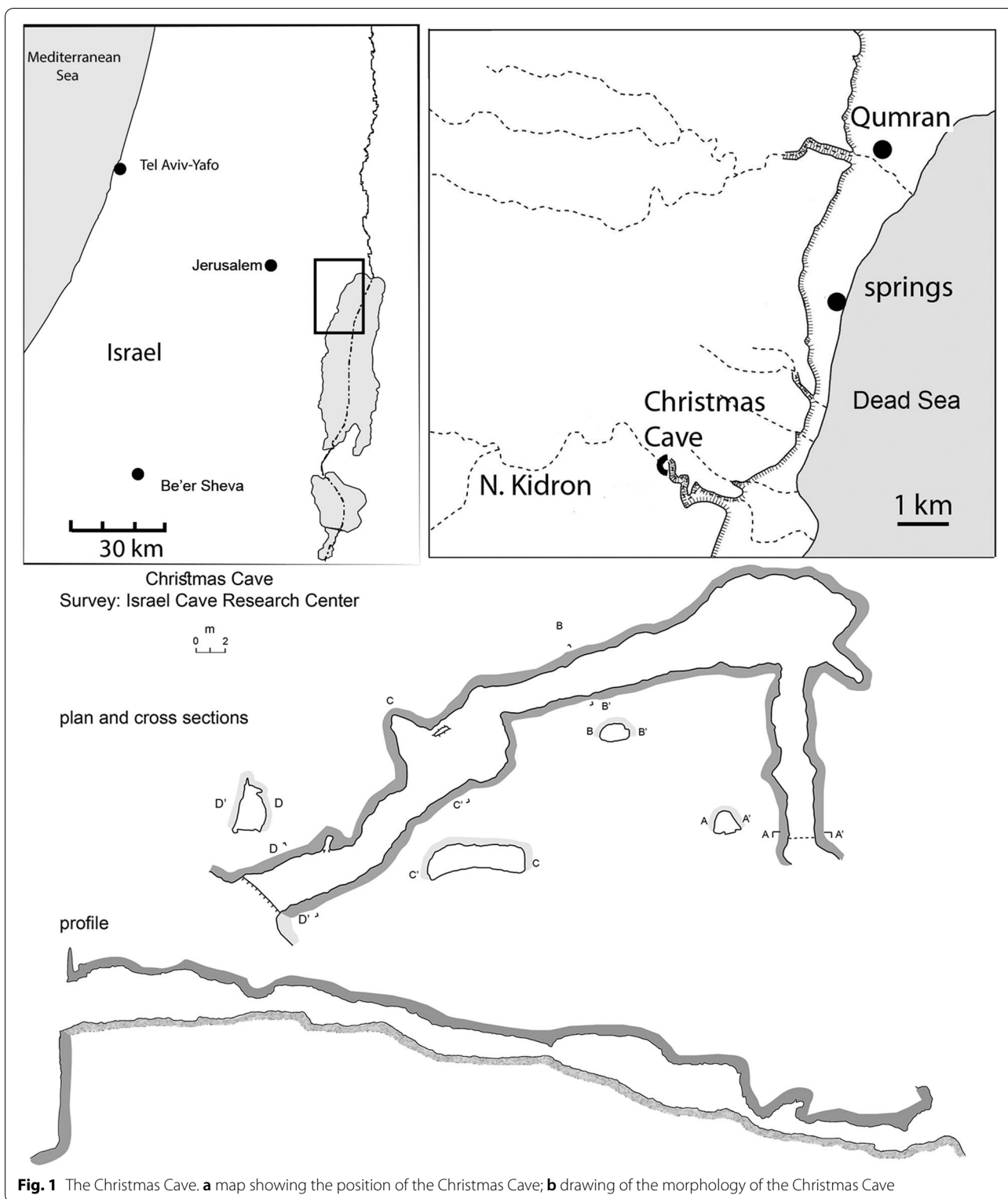


**Fig. 1** The Christmas Cave. **a** map showing the position of the Christmas Cave; **b** drawing of the morphology of the Christmas Cave

broad spectrum of colours including red, purple, black, blue, and green [11, 14], similar to other textiles from Roman sites in the Southern Levant (see for example [15, 16]) as well as all the textiles from all the Eastern provinces in the Roman Empire [17, 18]. Belis, Shamir, and Sukenik concluded that since no wool textiles were found in the Qumran Caves [19], and given other technological differences between the two assemblages, it was unlikely that the Christmas Cave inhabitants from the Roman period had any connection with Qumran. On the other hand, the Roman-period Christmas Cave textiles exhibit many similarities to the textile assemblage from the days of the First Jewish Revolt (66–73 CE) found at Masada, as well as to textile collections derived from other cliff caves in the Judean Desert, which served as refuge caves at the end of the Second Jewish Revolt.

While all this then appeared to confirm that the cave was used for refuge in the Bar Kokhba period, the question remained about how to date objects that were not classifiable by stratigraphy or typology to a particular period. How many different periods were represented in the cave?

Clearly, the papyrus pieces would most likely come from the Bar Kokhba period [3: 68–70]. Documents from this time, including some written by Bar Kokhba himself, have been found in the caves of Wadi Murabba'at, Naḥal Hever, and Naḥal Şe'elim ([20]:159–163; [21–25]: Table 3, 156–7). The small pieces of papyrus from the Christmas Cave appear consistent with such written materials, some of which are in Greek. To further define the epochs in which people visited, lived, or took refuge here, we present new investigations of several types of objects excavated in the Christmas Cave which will cast more light on precisely which periods saw occupation, what foodstuffs they ate, and what ceramic technology they possessed. For comparison, and further clarification, we will also qualify to what degree the Christmas Cave saw inhabitation simultaneously with the famous site of Qumran's main habitation in Periods I and II (from ca. 85 BCE to 68 CE).

## Materials

The materials investigated included textiles, reed, dung, plant stones, cereal grain, and ceramics. The 25 samples which have been investigated in the present study are listed in Table 1. In the following table, 'QCC' refers to the DSSF materials catalogued by EBAF in the 1980's, and is not the original listing system made by the British team. The designations "Frumkin" and "CC soil" indicate objects from the 2007 survey. All samples analysed were surface finds.

## Methods

### Radiocarbon dating

Samples of a variety of materials, rope, wood, charcoal, textile, wool, were dated by radiocarbon. Accelerator Mass Spectroscopy (AMS) dating was performed.

The samples underwent standard chemical pre-treatment AAA (Acid–Alkali–Acid), for cleaning and isolation of the datable fraction (see e.g. [26]). Next, the samples were combusted into CO<sub>2</sub> by an Elemental Analyzer (EA), coupled on-line with an Isotope Ratio Mass Spectrometer (IRMS). The EA is also used to purify the CO<sub>2</sub>. In addition, the EA/IRMS system enables precise measurements of the <sup>13</sup>C/<sup>12</sup>C-ratio. Part of the CO<sub>2</sub> is reduced to graphite by reacting under excess H<sub>2</sub> gas [27]. This graphite was pressed into target holders to be placed in the ion source of the AMS (Accelerator Mass Spectrometer). The AMS measured the <sup>14</sup>C/<sup>12</sup>C-ratio in the graphite.

Most samples were analysed in Groningen (laboratory code GrA). Five samples were analysed in Irvine (laboratory code UCI). The Groningen AMS facility is based on a 2.5 MV Tandetron accelerator [28].

The stable isotope ratio is expressed as a δ-values, defined as the deviation (expressed in per mil) of the rare to abundant isotope ratio from that of a reference material:

$$^{13}\delta = \left( \frac{(^{13}\text{C}/^{12}\text{C})_{\text{sample}}}{(^{13}\text{C}/^{12}\text{C})_{\text{reference}}} - 1 \right) \times 1000\text{‰}$$

The reference material is belemnite carbonate (V-PDB) [29]. The measured <sup>14</sup>C/<sup>12</sup>C-ratio was converted to a conventional Radiocarbon Age. The convention comprises the use of the Oxalic Acid standard, correction for isotopic fractionation and usage of the conventional half-life [30]. The measured activity ratios are reported in <sup>14</sup>a (%), 100% being the standard value. The conventional <sup>14</sup>C dates are calculated from these activity ratios and are reported in BP. The <sup>14</sup>C dates (in BP) need to be calibrated into calendar ages. This was done using the OxCal code [31] applying the most recent high-resolution calibration curve IntCal20 [32]. The calibration yields calendar age ranges, which are reported at both the 1σ and 2σ confidence level. All dates are rounded to 5.

### Thermoluminescence (TL) dating

TL-measurements were performed in Odense on a DA-12 TL-reader built by Risø National Laboratory in Denmark with the 100–300 μm granulometric fraction of sieved grains using a Single Aliquot Regeneration method adapted from Hong et al. [33], taking the average of four subsamples. No mineral separation has been

**Table 1** Samples analysed in the present study

KLR Lab No	GrA Lab No	QUM No	Field no	Sample description	Analyses performed
KLR-8008		430	QCC-007	Ceramic with fat	GC-MS, TS, TL, LA-ICP-MS, XRF, FT, SUS, FTIR, XRD
KLR-8009		426	QCC-079	Ceramic with fat	GC-MS, TL, LA-ICP-MS, XRF, SUS, FTIR, XRD
KLR-8010		428	QCC-264	Ceramic, blackened	TS, TL, LA-ICP-MS, XRF, FT, SUS, FTIR, XRD
KLR-8011		425	QCC	Ceramic, juglet, N trench I	TS, FT, SUS
KLR-8012		437	QCC-258	Ceramic, small juglet	GC-MS
KLR-8013	GrA-50530	437a	QCC-221	Dung	C14
KLR-8014	GrA-50531	427	III 1A	Charcoal	C14
KLR-8015	GrA-50532	436		Wood	C14
KLR-8016			QCC test s	Ceramic	GC-MS, TL, LA-ICP-MS, XRF, SUS, FTIR, XRD
KLR-8852	GrA-53282		C1	Cereal grain	C14
KLR-8853	GrA-53271		C2	Olive stone	C14
KLR-8854	GrA-53272		C3	Date stone	C14
KLR-8855	GrA-53273		C4	Reed	C14
KLR-8856	GrA-53274		C5	Textile	C14
KLR-8857			Frumkin#5	Ceramic	TS, TL, LA-ICP-MS, XRF, FT, SUS, FTIR, XRD
KLR-8858			Frumkin#6	Ceramic	TS, TL, LA-ICP-MS, XRF, FT, SUS, FTIR, XRD
KLR-8859			Frumkin#7	Ceramic	TS, TL, LA-ICP-MS, XRF, FT, SUS, FTIR, XRD
KLR-8860			Frumkin#11	Ceramic	TS, TL, LA-ICP-MS, XRF, FT, SUS, FTIR, XRD
KLR-8861			Frumkin#12	Ceramic	TS, TL, LA-ICP-MS, XRF, FT, SUS, FTIR, XRD
KLR-8862			Frumkin#15	Ceramic, lamp with soot	TS, TL, LA-ICP-MS, XRF, FT, SUS
KLR-8863			Frumkin#16	Ceramic	TS, TL, LA-ICP-MS, XRF, FT, SUS, FTIR, XRD
KLR-12527			CC1 soil	Soil from surface	LA-ICP-MS, XRF
KLR-12529			CC3 soil	Soil from surface	LA-ICP-MS, XRF
KLR-12530			CC4 soil	Soil from surface	LA-ICP-MS, XRF
KLR-12531			CC5 soil	Soil from surface	LA-ICP-MS, XRF

"QUM" are EBAF and J. Gunneweg numbers. GC-MS Gas Chromatography Mass Spectrometry, C14 Radiocarbon dating, TS Thin Section – petrographic description, FT Firing Temperature determination, TL Thermoluminescence, XRF X-Ray fluorescence, LA-ICP-MS Laser Ablation Inductively Coupled Plasma Mass Spectrometry, SUS magnetic susceptibility, FTIR Fourier Transform Infrared Spectroscopy, XRD X-ray diffraction

done. The calculation of the date required determining the dose received from the environment. This was assumed to originate from three sources: (1) the internal sources—from the four radioactive isotopes present in the samples,  $^{40}\text{K}$ ,  $^{232}\text{Th}$ ,  $^{235}\text{U}$ , and  $^{238}\text{U}$ ; (2) the external source—from the same four radioactive isotopes in the surrounding soil; and (3) the cosmic flux. The radioactive isotopes from the samples and the surrounding sediment were measured using LA-ICP-MS (for Si, Th and U) and XRF (for Si and K). The cosmic flux was estimated from the geographical position of the site, its altitude above sea level, the depth of finding and the density of the overlying sediment. The calculation was performed using the "Luminescence" package on R software [34]. The procedure required input of several parameters: (1) the self-shielding was calculated using a measured average density of  $1.8 \pm 0.3 \text{ g cm}^{-3}$ , (2) the grain diameter after sieving was assumed to be  $200 \pm 100 \mu\text{m}$ , (3) the alpha efficiency was assumed to be  $0.10 \pm 0.02$  according to Olley et al. [35], and (5) the sediment water content was estimated to be 2 wt%. No HF etching was performed;

thus, the alpha particle dose was included in the annual dose rate calculation [36]. These parameters were computed and processed through the AGE software [37] providing the dose rates and the TL-ages.

#### Laser ablation inductively coupled plasma mass spectrometry (LA-ICP-MS)

Laser ablation (LA) was performed with a CETAC LXS-213 G2 equipped with a NdYAG laser operating at the fifth harmonic at a wavelength of 213 nm. A 25  $\mu\text{m}$  circular aperture was used. The shot frequency was 20 Hz. A line scan was performed with a scan speed of  $20 \mu\text{m s}^{-1}$  and was ca. 300 s long following a 10 s gas blank. The helium flow was fixed at  $600 \text{ mL m}^{-1}$ . The laser operations were controlled by the DigiLaz G2 software provided by CETAC. Inductively coupled plasma mass spectrometry (ICP-MS) analyses were carried out using a Bruker Aurora M90 equipped with a frequency matching RF-generator. The basic parameters were as follows: radiofrequency power 1.30 kW; plasma argon gas flow rate  $16.5 \text{ L min}^{-1}$ ; auxiliary gas flow rate  $1.65 \text{ L min}^{-1}$ ; sheath



gas flow rate  $0.18 \text{ L min}^{-1}$ . The following isotopes were measured all without skimmer gas:  $^{29}\text{Si}$ ,  $^{232}\text{Th}$ , and  $^{238}\text{U}$ . No interference corrections were applied to the selected isotopes. The analysis mode used was peak hopping with 3 points per peak, and the dwell time was 10 ms on  $^{29}\text{Si}$  and 100 ms on  $^{232}\text{Th}$  and  $^{238}\text{U}$ . The quantification was performed with a method similar to that of Golitko and Terrell [38]. An in-house ceramic standard was run before and after batches of three samples in order to monitor the stability of the beam and to act as a standard. The concentration of U and Th were calculated by comparison of the U/Si and Th/Si experimental ratios to the U/Si and Th/Si standard material ratios. A relative error of ca. 10% is estimated from these measurements mostly due to mineral heterogeneity of the samples. For the analyses of other trace elements than U and Th, the same set was used, and the following isotopes were analysed for:  $^{55}\text{Mn}$ ,  $^{57}\text{Fe}$ ,  $^{59}\text{Co}$ ,  $^{65}\text{Cu}$ ,  $^{66}\text{Zn}$ ,  $^{75}\text{As}$ ,  $^{85}\text{Rb}$ ,  $^{88}\text{Sr}$ ,  $^{107}\text{Ag}$ ,  $^{111}\text{Cd}$ ,  $^{121}\text{Sb}$ ,  $^{205}\text{Tl}$ , and  $^{208}\text{Pb}$ . Here the analysis mode used was also peak hopping with 3 points per peak. The data were quantified by direct ratios to the count rates of the international standard material NIST612, which was analysed as every fourth sample.

#### Petrographic descriptions

Thin sections of  $30 \mu\text{m}$  thickness were manufactured from the ceramic samples in the Catamarca laboratory. They were polished with silicon carbide 80, 180, 400 and 600, photographed and described petrographically. Crossed polarized light (XPL) and plane polarized light (PPL) observations were done in a Leitz Ortholux polarizing microscope at 40X-100X. JMicrovision<sup>®</sup> software was used to make all the measurements and the point-counting analysis in each thin-section. A total of 300 points were recorded for each thin-section.

#### Magnetic susceptibility and TL-sensitivity measurements

The method of characterising clay sediments has proven effective in studies of provenancing archaeological ceramics, pot shards, and red brick. Magnetic susceptibility was measured using ca. 1 g samples with a KLY-2 susceptibility-metre capable of reaching ca.  $1 \times 10^{-6}$  SI-units. The thermoluminescence (TL) sensitivity was measured on four 10 mg aliquots of the crushed and sieved grain size fraction 100–300  $\mu\text{m}$ . For the TL-measurements a TL/OSL-system TL-DA-12 manufactured at Risø National Laboratory, Denmark was used. The palaeosignals were erased by heating the samples to  $400 \text{ }^\circ\text{C}$ . Subsequently the samples were irradiated for 60 s under a  $0.8 \text{ GBq } ^{90}\text{Sr}$ -source. The samples were then annealed for 30 s at  $200 \text{ }^\circ\text{C}$ , and the TL-signal measured from 202 to  $235 \text{ }^\circ\text{C}$  and integrated in order to yield the TL-sensitivity. Drift in photodetector high tension, optical transmission

and other system parameters were monitored by measuring four aliquots of a standard sample daily. The method and its application are described in [39–47].

#### Firing temperature determination

The maximum firing temperature was determined at University of Southern Denmark in the Odense laboratory by stepwise reheating as described in Rasmussen et al. [48]. This method was chosen over other methods such as e.g. the thermal expansion measurement method (see e.g. Tite [49]) as it is generally producing more reliable results. The samples were heated at 20 degrees steps starting from  $200 \text{ }^\circ\text{C}$  until  $1060 \text{ }^\circ\text{C}$ . The heating time was 24 h for the lowest temperatures, gradually decreased to 1 h with raising temperature. Upon cooling after each heating step, the samples were weighed and measured in quadruple for magnetic susceptibility on a KLY-2 Kappebridge manufactured by Geofyzika, Brno, with a detection limit of  $10^{-6}$  SI-units. The samples were all a factor of ca. 1000 times higher than the detection limit. A sample with known susceptibility was measured daily for absolute calibration. The empty sample holder was measured before and after each session and the average background susceptibility was subtracted from the actual measurements. The uncertainty was calculated from the four repeated measurements, between which the sample was turned in the sample holder. The reported uncertainties therefore to a large degree reflects the anisotropy of the sample. The firing temperature was read off a graph showing the squared first derivative of the susceptibility as a function of the reheating temperature [48].

#### Micro-X-ray fluorescence ( $\mu$ -XRF)

The embedded and polished samples were subjected to analysis by  $\mu$ -XRF for the quantification of K and Si. An ARTAX-800  $\mu$ -XRF situated at University of Southern Denmark and manufactured by Bruker-Nano was used and operated with a high tension of 50 kV and a current 600  $\mu\text{A}$ . Absolute calibration of the concentrations has been performed by the DCCR-method (Direct Calibration from Count Rates) provided by the Bruker software using the standard reference material NIST-2711.

#### Fourier Transform Infrared spectroscopy (FTIR)

The samples were analysed at University of Southern Denmark using a FTIR instrument (Agilent Technology, Cary 630) with a diamond crystal ATR accessory. Spectra were collected from 32 co-added scans in the spectral range  $4000\text{--}650 \text{ cm}^{-1}$  with a resolution of  $8 \text{ cm}^{-1}$ . The background was measured with 32 scans. The instrument was controlled through MicroLab software and data were processed with *Spectragryph* software (v.1.2.14 [50]). The second derivative of the spectra were calculated. This is

a widely used and useful method in FTIR studies for the identification of peaks barely visible in the raw spectra [51–56].

#### X-ray diffraction (XRD)

The XRD analyses were performed at the University of Southern Denmark using a PANalytical X'Pert PRO MPD system (PW3050/60) diffractometer with Cu K $\alpha$  radiation as the source ( $\lambda = 1.54 \text{ \AA}$ ) and a PIXcel3D detector. The X-ray generator was set to an acceleration voltage of 45 kV and a filament emission to 40 mA. All measurements were performed in continuous mode with a  $2\theta$  angle step size of  $0.026^\circ$  and a scan speed of  $0.022^\circ \text{ s}^{-1}$  in a range from  $5^\circ$  to  $90^\circ 2\theta$ . The qualitative analysis was performed using *Highscore Plus* software linked to the ICDD PDF-2 database.

#### Gas Chromatography Mass Spectroscopy (GC–MS)

GC–MS analysis was performed at the University of Pisa after extraction of grinded fragments of food crusts adhered to the internal surface of four ceramic vessels (KLR8008, KLR8009, KLR8012, and KLR8016) with  $\text{CH}_2\text{Cl}_2/\text{MeOH}$ . The extracts were dried and submitted to alkaline hydrolysis following a procedure described in the literature [57]. Particularly, the neutral (unsaponifiable) and the acidic fractions were obtained by extraction with hexane and, after acidification, with diethyl ether. Each fraction was derivatised with a silylating agent, N,O-Bis(trimethylsilyl)trifluoroacetamide (BSTFA), and separately analysed by GC–MS.

## Results

### Radiocarbon dating

The radiocarbon dates acquired in this study are listed in Table 2. The columns are the laboratory identification numbers, the  $^{14}\text{C}$  activities and measurement uncertainties, the Carbon content (C%) of the analysed sample

materials, the  $\delta^{13}\text{C}$  values, the  $^{14}\text{C}$  ages in BP and the calibrated age ranges in CE/BCE, both  $1\sigma$  and  $2\sigma$ . The  $^{14}\text{C}$  dates and calibrated dates are rounded to 5 years. Multiple calibrated ranges are taken together.

### TL-datings

The Si, K, U, and Th concentrations and the TL-dates are listed in Table 3. Both  $1\sigma$  and  $2\sigma$  uncertainty ranges are listed, and both intervals are used in the discussion below. Results for 4 soil samples later procured by Amos Frumkin are listed below the samples in Table 3 (one additional soil sample failed to yield usable results for Si and was therefore discarded). Below this is listed the average soil composition together with a  $1\sigma$  uncertainty calculated as 10% of the concentration values. The latter is a best estimate, based mainly on an assessment of the inhomogeneity of the soil samples. The radiation contribution from the soil is applied as half the calculated average soil composition, because the ceramic samples were assumed to have been residing on the floor of the cave, not dug down into the chalkstone.

### Petrographic and mineralogical analysis of the ceramic samples

The results of the XRD and FTIR analysis (Table 4) confirmed the mineralogical observations and brought some complementary information. FTIR second-derivative spectra and XRD diffractograms, as well as the results of the firing temperature determinations are available in Additional file 1.

Secondary calcite was identified in some sherds, and here the combination of petrography and the results of the FTIR show the presence of primary calcite (KLR-8010, KLR-8859, KLR-8861, KLR-8862, and KLR-8863). In the felsic minerals, XRD and FTIR revealed the presence of quartz and several potassium and plagioclase series feldspars. The XRD patterns point to the presence

**Table 2** Results of the radiocarbon dating

KLR lab No	GrA lab No	$\delta^{13}\text{C}$ (‰)	Sample material	C%	$^{14}\text{a}$ (%)	$\sigma^{14}\text{a}$	Age (BP)	Calibrated age range ( $1\sigma$ )	Calibrated age range ( $2\sigma$ )
8853	53271	−20.94	Olive stone	48.8	92.21	0.38	$650 \pm 35$	CE1290–1390	CE 1280–1400
8854	53272	−23.41	Date stone	46.0	79.71	0.34	$1820 \pm 35$	CE 170–325	CE 125–330
8013	50530	−24.45	Macro remains	35.1	79.42	0.38	$1850 \pm 40$	CE 130–240	CE 80–325
8856	53274	−25.11	Textile	39.9	78.82	0.33	$1910 \pm 35$	CE 80–205	CE 25–220
8855	53273	−23.99	Reed	43.4	78.44	0.33	$1950 \pm 35$	CE 25–125	BCE 40–CE 205
8015	50532	−24.78	Wood	48.4	78.30	0.37	$1965 \pm 40$	BCE 5–CE 120	BCE 50–CE 205
8014	50531	−22.11	Charcoal	75.6	52.57	0.28	$5170 \pm 40$	BCE 4045–3950	BCE 4160–3805
8852	53282	−22.63	Cereal grain	35.0	51.86	0.25	$5275 \pm 40$	BCE 4230–3995	BCE 4240–3985

The columns show KLR and GrA laboratory code numbers,  $\delta^{13}\text{C}$  in ‰, sample material,  $^{14}\text{C}$  activity ratio corrected for isotope fractionation in ‰, its standard deviation,  $^{14}\text{C}$  age in BP including its standard deviation, and calibrated age ranges in BCE at  $1\sigma$  and  $2\sigma$  confidence intervals. The  $^{14}\text{C}$  dates are calibrated with the latest calibration curve IntCal20 [32]. See text for details

**Table 3** Results of the TL-dating of the ceramic samples

Lab No	Code	Field no	Si wt%	K wt%	U µg/g	Th µg/g	Date BCE/CE	1σ	1σ interval	2σ interval
KLR-8008	QCC-430	QCC-007	25.1	1.14	2.32	4.92	450 CE	100	350–550 CE	250–650 CE
KLR-8009	QCC-426	QCC-079	30.4	1.71	1.84	6.33	334 CE	106	228–440 CE	122–546 CE
KLR-8010	QCC-428	QCC-264	8.63	1.91	1.53	1.86	3208 BCE	354	3563–2854 BCE	3916–2500 BCE
KLR-8016		?	24.5	1.58	1.43	5.35	413 BCE	155	568–258 BCE	723–103 BCE
KLR-8857		Frumkin#5	29.3	1.51	2.15	8.60	59 BCE	127	186 BCE – 70 CE	313 BCE–195 CE
KLR-8858		Frumkin#6	31.8	1.58	2.99	10.9	240 CE	110	130–350 CE	20–460 CE
KLR-8859		Frumkin#7	19.0	3.55	1.87	4.05	476 CE	107	369–583 CE	262–690 CE
KLR-8860		Frumkin#11	22.1	4.17	2.37	5.85	698 BCE	206	904–492 BCE	1110–286 BCE
KLR-8861		Frumkin#12	17.3	4.14	2.46	4.02	92 BCE	142	234 BCE – 50 CE	376 BCE–192 CE
KLR-8862		Frumkin#15	10.6	2.67	3.72	3.98	145 BCE	151	296 BCE – 6 CE	447 BCE–157 CE
KLR-8863		Frumkin#16	22.2	1.15	2.24	6.68	272 BCE	180	456–92 BCE	632 BCE–88 CE
KLR-12527		CC1 soil	3.99	2.87	1.085	0.495				
KLR-12529		CC3 soil	0.165	1.93	0.098	0.021				
KLR-12530		CC4 soil	0.325	1.49	0.476	0.049				
KLR-12531		CC5 soil	0.230	3.38	0.268	0.046				
Average		soil	1.18	2.42	0.482	0.153				
1σ (10%)			0.12	0.242	0.048	0.015				

A sample called CC2-soil was available but did not contain quantifiable amounts of Si by XRF and were consequently left out

**Table 4** Mineral phases identified by XRD and FTIR analyses

Samples	XRD										FT-IR										
	Qz	Cal	K-fs	An	Al	Hem	Grt	Gh	Di	Wo	Qz	Cal	Cal 2nd	An	Al	Or	Mc	Sn	Gh	Di	Wo
KLR-8008	xxxx	–	xx	XX	–	x	–	–	–	–	xxx	x	x	xx	xx	xx	–	x	x	–	–
KLR-8009	xxxx	–	xx	xxx	xx	xx	–	–	–	–	xxxx	–	xx	xx	x	–	x	x	x	–	x
KLR-8010	xxx	xxx	xx	XX	x	–	x	–	–	x	xx	xxxx	–	xx	x	x	x	x	x	x	–
KLR-8016	xxx	xx	xx	xx	–	xx	–	–	x	–	xxx	x	x	xx	–	–	xx	–	xx	x	xx
KLR-8857	xxxx	xx	xx	xx	x	xx	–	x	–	–	xxx	xx	x	xx	xx	x	xx	x	xx	x	–
KLR-8858	xxxx	x	xx	xx	xx	xx	–	–	–	–	xxx	xx	xx	xx	x	x	–	x	xx	x	xx
KLR-8859	xxx	xxx	xx	x	–	xx	–	–	x	–	xxx	xx	x	xx	xx	x	–	–	xx	x	–
KLR-8860	xxx	x	xxx	–	x	xxx	–	–	x	–	xxx	x	xx	x	x	x	–	x	xx	x	xx
KLR-8861	xxx	xxxx	xxx	x	–	–	–	–	–	x	xxx	xx	x	xx	x	xx	–	x	xx	–	–

of a moderate amount of potassium feldspars, including three sherds with sanidine (KLR-8859, KLR-8860, and KLR-8861), while the FTIR data give more information about the potassium feldspars, showing the presence in most of the sherds of orthoclase and sanidine, and, in some sherds, microcline. Concerning the plagioclase series, the presence of two specific feldspars was observed: anorthite and albite, anorthite being the most common plagioclase mineral. Various amounts of gehlenite, wollastonite, and diopside have been detected in all the sherds. These neo-formation minerals have been

detected by both instrumental techniques, but the FTIR second-derivative method appears to be more sensitive than the XRD. Iron oxides such as hematite were identified in at least four of the sherds (KLR-8008, KLR-8009, KLR-8858, and KLR-8861).

The absence of clay minerals (such as illite, smectite, and kaolinite) in the XRD and FTIR analyses indicated that the pottery was fired above 500–550 °C. As most of the pottery analysed is Ca-based ceramics, the presence of several neo-formation mineral phases in the



fabrics was expected. The presence of wollastonite, a neo-formed mineral at the carbonate-quartz interface, indicates firing temperatures as high as 850–900 °C or above (sherds KLR-8009, KLR-8010, KLR-8016, KLR-8858, and KLR-8860). The presence of diopside and gehlenite indicate temperatures mostly above 750–800 °C, and gehlenite mostly is a good indicator of temperatures above 800 °C, although it starts to nucleate at 650 °C. The presence of microcline together with orthoclase in one sherd suggest firing temperatures not above 750 °C (KLR-8857). The absence of relevant peaks of calcite in the XRD patterns in some of the sherds and the presence of neo-formation mineral phases suggest firing temperatures in the range of 900–950 °C (KLR-8860 and KLR-8858) (see Additional file 1).

The ceramic samples are mostly characterized by presence of very fine or fine quartz-grained fabrics. The matrices are generally isotropic (i.e., not optically active) and most of them are formed by aggregates and very fine-grained quartz (Fig. 2 and Additional file 1). Only one sherd (KLR-8859) presented an anisotropic matrix formed by mica (biotite) in addition to very fine-grained quartz. Most of the sherds have an average of 14.4% inclusions, 78.8% matrix and 6.8% voids. The common primary minerals identified are quartz (and polycrystalline quartz), plagioclase feldspar, and calcite (mostly secondary). Accessory minerals identified are pyroxene, amphibole (brown hornblende), and some opaque minerals. Additionally, some rock fragments (mostly igneous rock fragments, granite) were identified at trace level. One exception was sample KLR-8810, which features abundant large granite fragments. Sample KLR-8858 also presents fragments of limestone (sedimentary rock) at trace levels. Generally, mineral inclusions and voids are evenly distributed. According to the mineral assemblages recorded by optical microscopy on thin-sections, the investigated sherds can be classified into 7 petrographical fabrics:

- Fabric 1: KLR-8008 (rounded quartz, probably coming from fluvial deposits).
- Fabric 2: KLR-8010 (a very distinctive shard, with mineralogy characterized by very fine/fine quartz inclusions + large igneous rock fragments of granite type).
- Fabric 3: KLR-8858 (high percentage of argillaceous inclusions + very fine quartz).
- Fabric 4: KLR-8857, and KLR-8009 (very fine quartz + plagioclase with a good distribution and a selection of temper).
- Fabric 5: KLR-8860 (very fine low sphericity quartz + plagioclase; presence of grog).
- Fabric 6: KLR-8861 and KLR-8863 (high percentage of primary and secondary calcite). KLR-8859 (very fine quartz + argillaceous inclusions + grog).
- Fabric 7: KLR-8862 (high percentage of primary and secondary calcite + argillaceous inclusions).

#### Trace elements and magnetic susceptibility versus TL-sensitivity

The trace elements compositions determined by LA-ICP-MS, the magnetic susceptibility, and the TL-sensitivity results are all listed in Table 5.

In the magnetic susceptibility versus TL-sensitivity cross plot (Fig. 3), the ceramics studied here are compared to 12 ceramic sherds from Qumran [42]. More than half of the samples from Qumran are gathered in the top-left corner of the plot with high to moderate magnetic susceptibility and low TL-sensitivity. The sherds from the Christmas Cave are more widely spread on the plot. Most of them seem to exhibit a higher TL-sensitivity than the Qumran ceramics indicating a difference in the raw materials used for the fabrication of the ceramics in Qumran and in those found in the Christmas Cave.

To achieve a better distinction between the samples, the trace elements data were processed using multivariate technique. Because of the low number of sample and the higher number of variables ( $p > n$ ), the use of Sparse PCA (SPCA) is more suited than regular PCA and eases the interpretation of the cross plot. The cross plot (Fig. 4) was computed with the R package “SparseBiplots” [58] using the LASSO method [59] with  $\lambda = 0.22$ . The results show that the 52% of the variation is explained by PC1 (principal component 1) and 22% is explained by the PC2. There are strong contributions of Co, Fe, Sb, and Ni aligned with PC1, whereas Zn, Ag, Pb, and Mn are aligned with the PC2. Arsenic, Cd, Tl, and Sr are contributing to both PC1 and PC2. Six samples are located on the left side of the biplot with negative coordinates on PC1 (KLR-8857, KLR-8859, KLR-8860, KLR-8861, KLR-8862, and KLR-8863). The three samples KLR-8008, KLR-8010, and KLR-8858 are separate from these with positive PC1 values. The comparison between the chemical results and the petrological fabrics is consistent even if several petrological fabrics are gathered in the same area to the left in the SPCA cross plot.

#### Analyses of organic residues

The results of the GC-MS analyses of organic material associated with the pottery fragments are shown in Fig. 5. Peak assignments are listed in Tables 6 and 7.

The results highlight a complex pattern of mono- and di-carboxylic fatty acids (Fig. 5a and c) in all the four

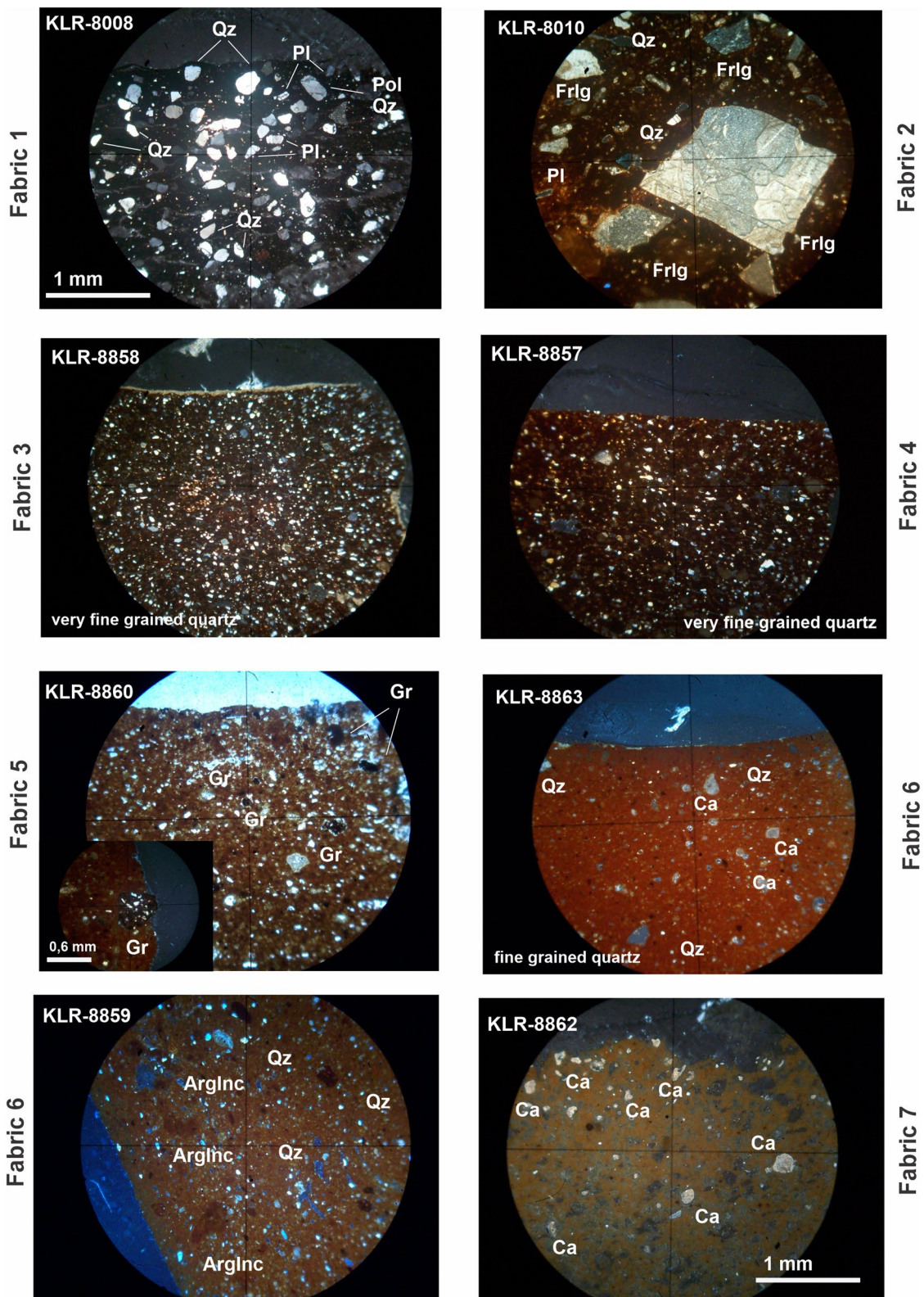


**Fig. 2** Microphotographs of six sherds in crossed polarized light (XPL) showing the main mineral and rock fragment inclusions for six of the seven defined petrographic groups (40X)

**Table 5** Results of the trace element concentrations determined by LA-ICP-MS

	Mn μg g <sup>-1</sup>	Fe wt%	Co μg g <sup>-1</sup>	Ni μg g <sup>-1</sup>	Cu μg g <sup>-1</sup>	Zn μg g <sup>-1</sup>	As μg g <sup>-1</sup>	Rb μg g <sup>-1</sup>	Sr μg g <sup>-1</sup>	Ag μg g <sup>-1</sup>	Cd μg g <sup>-1</sup>	Sb μg g <sup>-1</sup>	Tl μg g <sup>-1</sup>	Pb μg g <sup>-1</sup>	SUS 10 <sup>-3</sup> SI	1σ 10 <sup>-3</sup> SI	TL-235 Arb	1σ Arb
KLR-8008	1146	4,35	27,8	144,9	46,4	245,8	13,4	49,3	252	2,09	0,528	1,97	0,623	353	10,0	0,01	1,30	0,45
KLR-8010	678	6,19	22,3	124	99,8	n.d	19,5	53,9	673	0,259	1,71	1,24	3,25	6,05	7,34	0,07	0,550	0,13
KLR-8857	787	4,44	19,4	59,3	29,5	90,9	11,2	51,0	109	0,367	0,116	0,401	0,304	12,0	25,8	0,02	11,3	1,40
KLR-8858	1751	6,37	38,0	87,0	44,0	124	6,05	81,2	148	0,533	0,165	0,912	0,558	19,7	26,1	0,13	6,28	0,74
KLR-8859	562	4,77	19,2	53,4	29,7	101	12,8	96,2	373	0,307	0,446	0,600	0,686	17,3	7,13	0,05	0,740	0,31
KLR-8860	486	4,49	19,1	43,1	23,5	112	15,3	93,6	194	0,194	0,220	0,588	0,509	15,0	32,5	0,86	0,950	0,40
KLR-8861	197	2,32	9,33	20,6	14,7	64,3	6,97	62,6	167	0,270	0,107	0,298	0,329	7,86	3,69	0,02	0,330	0,41
KLR-8862	465	2,98	13,8	46,7	31,8	168	7,59	71,5	270	0,271	0,097	0,442	0,0333	13,2	17,1	0,01	2,03	0,74
KLR-8863	451	3,69	16,2	33,3	21,2	96,5	13,3	96,6	254	0,350	0,151	0,499	0,557	17,0	14,2	0,02	0,520	0,15

Iron is given in wt%, the rest of the trace elements in μg g<sup>-1</sup>, the relative standard deviation is ca. 15%. Also listed is magnetic susceptibility (SUS), which is measured in 10<sup>-3</sup> SI units, and the TL-sensitivity (TL-235) measured in arbitrary units as described in [41]

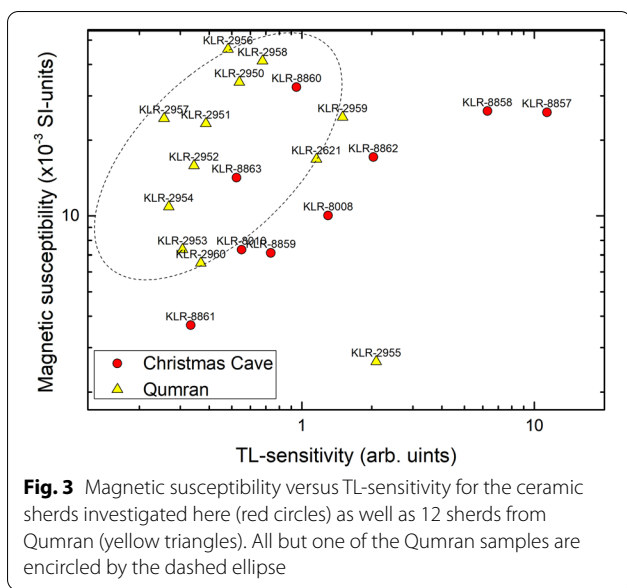


**Fig. 3** Magnetic susceptibility versus TL-sensitivity for the ceramic sherds investigated here (red circles) as well as 12 sherds from Qumran (yellow triangles). All but one of the Qumran samples are encircled by the dashed ellipse

samples analysed by GC–MS: glycerolipids are the main component of the vessel lipids. The use of calibration curves for the linear fatty acids allowed us to perform an estimation of the lipid content, which was above 50 µg for samples KLR-8009 and KLR-8012 and above 120 µg for sample KLR-8008 and KLR-8016 (the quantitation limit, based on procedural blanks, is ca. 3 µg). In particular, the

acidic fractions of the saponified extracts were showed to contain even and odd chain saturated linear mono-carboxylic fatty acids, with 8–24 carbon atoms in the acyl chain, with hexadecanoic acid (palmitic acid, peak #30) and octadecanoic acid (stearic acid, peak #41) as the most abundant. The fatty acid profiles also featured variable amounts of the unsaturated *cis* and *trans* octadecenoic acid isomers (oleic and elaidic acids, peaks #39 and 40), particularly abundant in samples KLR-8012 and KLR-8016.

The neutral fraction of sample KLR-8008 features a relevant amount of long chain ketones (Fig. 5b, peaks #26, 29–39 in the neutral fraction). Finally, some plasticizers (*i.e.*, phthalates) were also detected.

Table 8 summarizes the identified compounds and materials for all the four samples analysed.

### Discussion

#### Dating and occupational phases

The collective set of radiocarbon dates and TL-dates from the present study and previous studies shows that the Christmas Cave has been temporarily used in several episodes during the last 6500 years (Figs. 6 and 7; Table 9).

A single early fifth millennium BCE radiocarbon date (GrA-24265) was made on wood. However, it is undetermined if it should be taken to represent an early

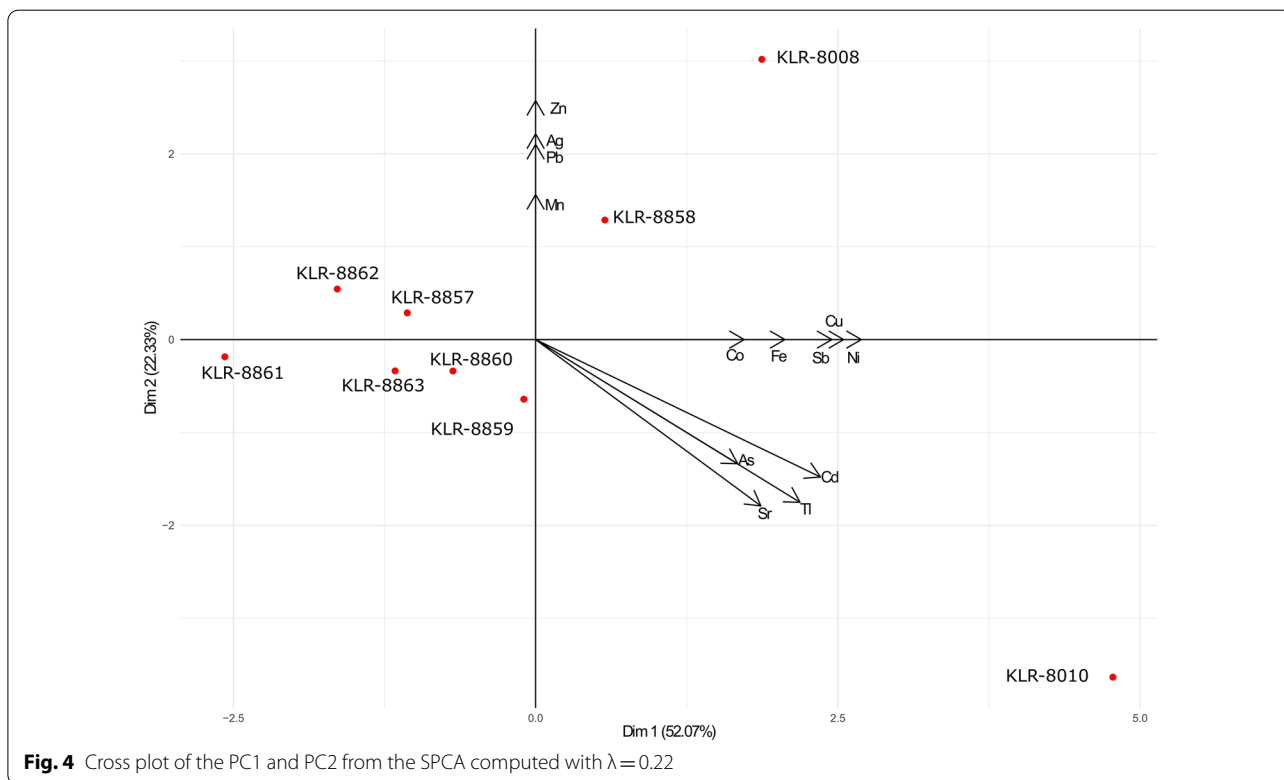
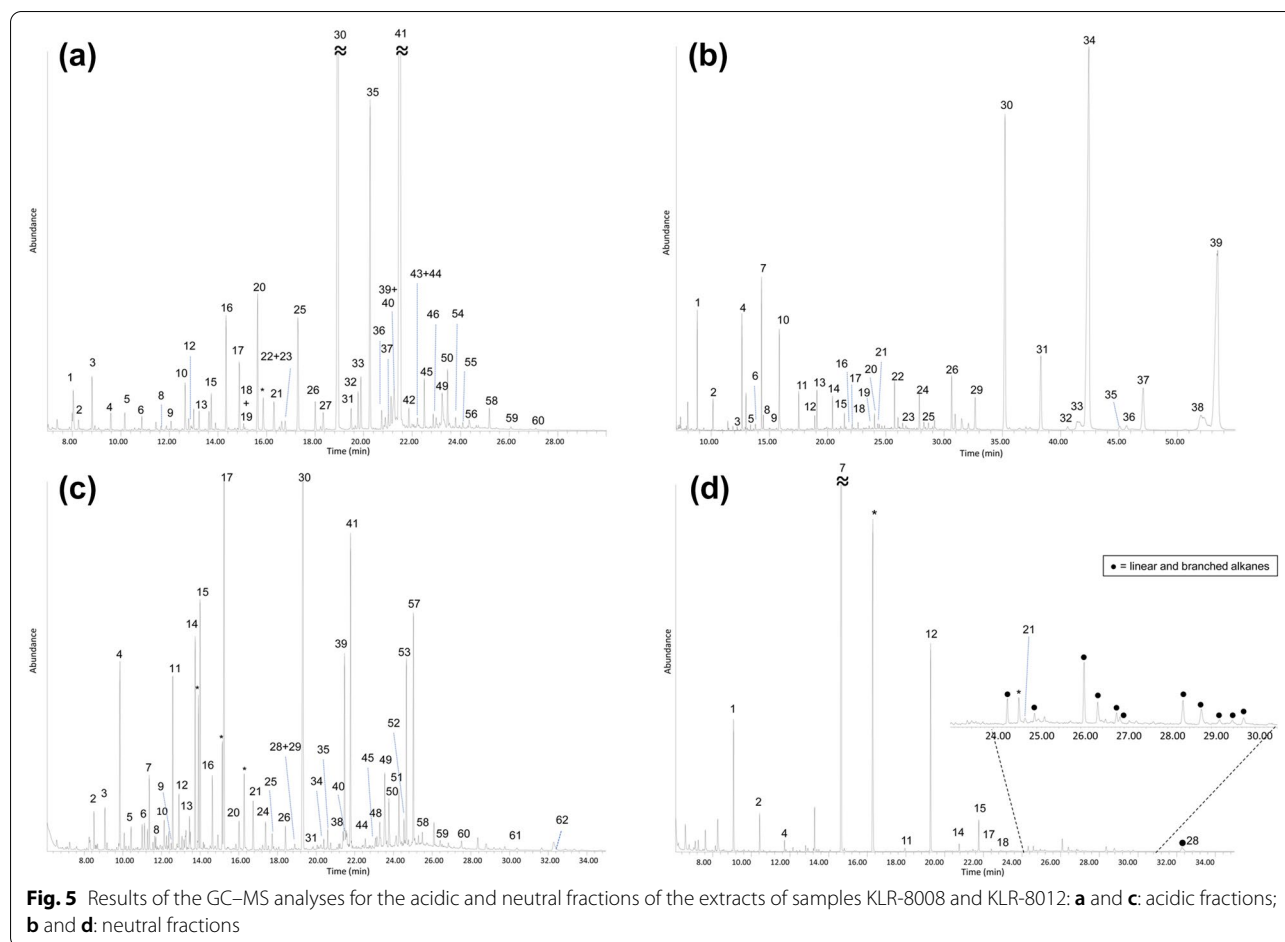


**Fig. 4** Cross plot of the PC1 and PC2 from the SPCA computed with  $\lambda=0.22$





Chalcolithic use of the cave, or whether the wood was re-used at a later time. In any case, no clear archaeological evidence for an early fifth millennium phase was attested in the material record otherwise from the cave, or elsewhere in the Judean Desert caves to date ([60]: 172), which strongly suggests that old wood was used by the occupants at an unknown time thereafter.

The cave was certainly occupied in the Late Chalcolithic, during the last quarter of the fifth millennium BCE. This is indicated by three radiocarbon dates from a cereal grain and two pieces of charcoal (KLR-8852/GrA-53282, KLR-5464/GrA-24261, KLR-8014/GrA-50531, see Tables 2 and 9). This is in accordance with the archaeological evidence in the form of a small yet typical Late Chalcolithic pottery assemblage ([60]: 381–384, Fig. 33.4). It is likely that some of the 71 linen fragments from the DSSF excavation classified by Shamir and Suke-nik as “Chalcolithic” [11, 14] also belong to this phase according to the splicing technique that were observed in those textiles ([61]: 34).

A second late prehistoric habitation phase is attested by three radiocarbon dates and one TL-date from pieces

of textile and a ceramic fragment (samples KLR-10430/GrA-65501, UCI-79817, UCI-79815, and KLR-8010). The three radiocarbon dates are clustered around 3630–3530 BCE, a time span currently associated with the Early Bronze Age 1A in the conventional South Levantine chronology (e.g., [62, 63]: 26–43). Activity during this time span is virtually unknown from the Judean Desert [64], with only one other radiocarbon date thus far obtained from the region (the latest date from the “Cave of the Warrior” in Wadi al-Makkukh; [65]: sample RT-1943). There has not yet been found independent archaeologically dated materials from the Christmas Cave from Early Bronze Age 1A, although it is possible that some of the textiles previously classified as “Chalcolithic” may belong to this phase.

Approximately two thirds of the radiocarbon and TL dates fall between 45 BCE and 320 CE ( $2\sigma$ ). A single date from an olive stone (KLR-8853/GrA53271) is medieval, 1280–1395 CE, which falls in the early Mamluk period and testifies to a visitor from this time. A single TL-date (KLR-8860, Table 3) falls in the late Iron Age, or First Temple Period, around 700 BCE.



**Table 6** Peak assignment for the GC–MS chromatograms of the acidic fractions of samples KLR-8008 and KLR-8012 in Fig. 6

Peak #	Retention time (min)	Peak assignment
1	8.0	Benzoic acid
2	8.3	Octanoic acid
3	8.8	Tridecane
4	9.6	Nonanoic acid
5	10.2	Tetradecane
6	10.9	Decanoic acid
7	11.4	Heptanedioic acid, 1-methyl ester
8	11.7	Hexanedioic acid
9	12.1	Undecanoic acid
10	12.7	Hexadecane (IS1)
11	12.6	Octanedioic acid, 1-methyl ester
12	12.8	Heptanedioic acid
13	13.2	Dodecanoic acid
14	13.7	Octanedioic acid, 1-methyl ester
15	13.7	Octanedioic acid
*	13.9	Phthalic acid
16	14.3	Tridecanoic acid (IS2)
*	15.1	Terephthalic acid
17	14.9	Nonanedioic acid
18	15.0	$\omega$ -hydroxy-decanoic acid
19	15.1	Tetradecanoic acid (br)
20	15.6	Tetradecanoic acid
*	15.9	Phthalate (contaminant)
21	16.3	Decanedioic acid
22	16.6	Pentadecanoic acid (br)
23	16.8	Pentadecanoic acid (br)
24	17.4	Hexadecanoic acid, methyl ester
25	17.3	Pentadecanoic acid
26	18.0	Undecanedioic acid
27	18.3	Hexadecanoic acid (br)
28	18.8	(Z)-9-hexadecenoic acid
29	19.0	(E)-9-hexadecenoic acid
30	18.9	Hexadecanoic acid
31	19.5	Dodecanedioic acid
32	19.8	Heptadecanoic acid (br)
33	19.9	Heptadecanoic acid (br)
34	20.4	Octadecanoic acid, methyl ester
35	20.3	Heptadecanoic acid
36	20.7	Tridecanedioic acid
37	21.0	Octadecanoic acid (br)
38	21.4	9,12-octadecadienoic acid
39	21.1	(Z)-9-octadecenoic acid
40	21.7	(E)-9-octadecenoic acid
41	21.5	Octadecanoic acid
42	21.9	Tetradecanedioic acid
43	22.2	Nonadecanoic acid (br)
44	22.5	Hydroxycarboxylic FA -TMS
45	22.5	Nonadecanoic acid

**Table 6** (continued)

Peak #	Retention time (min)	Peak assignment
46	22.8	Pentadecanedioic acid
47	23.0	$\omega$ -hydroxyhexadecanoic acid
48	23.3	Unknown (73, 129, 227, 329)
49	23.5	10-oxo-octadecanoic acid
50	23.5	eicosanoic acid
51	24.3	9,x-dihydroxyoctadecanoic acid (?)
52	24.5	9,x-dihydroxyoctadecanoic acid (?)
53	24.6	9,x-dihydroxyoctadecanoic acid (?)
54	23.8	Hexadecanedioic acid
55	24.0	$\omega$ -hydroxyoctadecanoic acid
56	24.4	Heneicosanoic acid
57	25.0	9,x-dihydroxyoctadecanoic acid (?)
58	25.2	Docosanoic acid
59	26.1	Tricosanoic acid
60	27.0	Tetracosanoic acid
61	30.4	Hexacosanoic acid
62	32.3	Cholesterol (traces)

All organic acids and alcohols are detected as their TMS esters and ethers, respectively

The calibrated date intervals ( $1\sigma$  and  $2\sigma$ ) between 500 BCE and 500 CE are depicted in Fig. 7, which also shows three rectangles indicating the main habitation period for the Qumran settlement (ca. 100 BCE to 68 CE; ignoring the Roman occupation after 68 CE), the First Jewish Revolt (66–73 CE), and the Second Jewish Revolt or the reign of Bar Kokhba (132–136 CE).

There are six radiocarbon dates with  $1\sigma$  ranges in-between the two revolts, i.e., from 73 to 132 CE. However, if the  $2\sigma$  ranges are considered, multiple radiometric and TL dates overlap with both the Qumran Main Habitation period and the Second Jewish Revolt. So, the temporal resolution in the dates available is not sufficient to resolve with certainty if the Christmas Cave was visited during both or only one of the revolts, or indeed in the time between the revolts.

Pottery from the Hasmonean era (2nd to first century BCE) may be linked with the nearby harbour of Khirbet Mazin, at the mouth of the Wadi Qidron, which was established in the time of Alexander Jannaeus (ca. 85 BCE) and continued to be in use through the Early Roman period (see [66]: 77–78; [67]: 18–29; [68]). The Hasmoneans also re-used old Iron Age sites in the nearby Buq'ah (see [69]: 145). North of the Lower Qidron valley there was a track leading from the Dead Sea through the wilderness to Bethlehem and Jerusalem, thus travellers in peacetime could also have made use of the caves temporarily.

The TL-dates of ceramic fragments from the 4th to sixth centuries are consistent with what we know of

**Table 7** Peak assignment for the GC/MS chromatograms of the neutral fractions of samples KLR-8008 and KLR-8012 in Fig. 6

Peak #	Retention time (min)	Peak assignment
1	8.8	Tridecane
2	10.2	Tetradecane
3	12.2	Dodecane
4	12.7	Hexadecane (IS1)
5	13.4	1-tridecanol
6	13.8	Heptadecane
7	14.3	Tridecanoic acid (IS2)
8	14.5	1-tetradecanol
9	15.6	1-pentadecanol
10	15.9	Phthalate (contaminant)
11	17.5	1-hexadecanol
12	18.9	Hexadecanoic acid
13	19.1	1-heptadecanol
14	20.4	1-octadecanol
15	21.5	Octadecanoic acid
16	21.6	1-nonadecanol
17	22.1	Tricosane
18	22.6	1-eicosanol
19	23.6	1-eneicosanol
20	24	Pentacosane
*	24.3	Phthalate (contaminant)
21	24.4	1-docosanol
22	25.7	Heptacosane
23	26.1	1-tetracosanol
24	27.9	Octacosane
25	28.4	1-hexacosanol
26	30.6	Nonacosan-14-one
27	32.4	Cholesterol
28	32.7	Triacontan-15-one
29	35.2	Hentriacontan-16-one
30	38.3	Dotriacontan-16-one
31	40.6	Tritriacontanone
32	42.3	Tritriaconten-16-one
33	41.4	Tritriacontan-16-one
34	45.1	Tetratriacontanone
35	45.7	Tetratriacontanone
36	47.1	Tetratriacontan-16-one
37	52	Pentatriaconten-18-one
38	53.4	Pentatriacontan-18-one

All organic acids and alcohols are detected as their TMS esters and ethers, respectively

Byzantine hermits who lived in desert caves during this time (KLR-8008, 8009, 8858, and 8859). The Byzantine sample KLR-8008 is special, because it is a sample containing thermally altered fats, it has a specific fabric type (1), and it is the sample with the highest percentage of voids and the highest percentage of quartz. Also, it plots

distinctly different from the Qumran samples in the provenancing plot (Fig. 4).

Apart from the one Bronze Age TL-date, the other TL-dates are rather uniformly spread out from 700 BCE to 475 CE. Three TL-dates are overlapping the main habitation period of Qumran (ca. 100 BCE to 68 CE) with the  $1\sigma$  interval (KLR-8857, 8861, and 8862). One TL-date overlaps the Second Revolt period in the  $1\sigma$  interval (KLR-8858).

### The ceramics

It is evident from the archaeological evidence of the site that none of the ceramics found in the Christmas Cave were produced close by. The ceramic samples exhibit traits that can trace their place of origin, although they cannot be provenanced to any specific location, at least not from the present study. The analyses of the ceramics show some differences in the resources used for their manufacture, which again might indicate differences in location of origin of the people seeking shelter or refuge in the cave.

From a technological point of view, the pottery found in the Christmas Cave was made using different recipes by ancient potters. Two main *momentums* can be defined. The oldest sherds (KLR-8010, 8860, 8861, 8862, and 8863) are characterized by ceramic pastes with poorly sorted minerals and very low grain selection; low firing temperatures are very characteristic in these early shards as indicated by the presence of primary calcite. Surprisingly, the presence of grog which was found in only one shard (KLR-8860) indicates something more than routine recipes for the making of the pottery. This practice should be fully investigated further in the future. One of the older sherds, KLR-8010, was found to have a relative high firing temperature. The younger sherds (KLR-8857, 8858, 8008, and 8859) are characterised by well sorted mineral grains and an excellent grain selection used to elaborate the ceramic pastes. Most of them are very fine quartz tempered with low percentages of voids, indicating a very elaborated recipe to make the vessels.

Summarizing the inorganic measurements of the ceramic material it appears that there are probably four different sources for the raw materials of the ceramics. Ceramics were fired at temperatures well above 600°C, reaching 800–850°C for some of them. Several neo-formation mineral phases were identified by XRD and FTIR. The results of the LA-ICP-MS and the mineralogy analysis seen through the SPCA analysis (Fig. 4) suggest that the samples KLR-8008, KLR-8010 and KLR-8858 are possibly from three different locations. The six samples KLR-8857, KLR-8859, KLR-8860, KLR-8861, KLR-8862, and KLR-8863 group together which might indicate that they share a common origin. The three samples KLR-8861, 8862 and 8857 are probably contemporary with Qumran,

**Table 8** Results of the GC–MS analyses of the organic fraction extracted from four ceramic samples

Sample	Identified compounds	Identified material
KLR-8008	Mono-, hydroxy- and di-carboxylic fatty acids (linear and branched). Long chain linear and branched alcohols and alkanes/alkenes. Long chain ketones	Oxidised glycerolipids of animal and plant origin, plant waxes. Lipid Material submitted to heating
KLR-8009	Mono-, hydroxy- and di-carboxylic fatty acids (linear and branched). Long chain linear and branched alcohols and alkanes/alkenes	Oxidised glycerolipids of animal and plant origin, plant waxes
KLR-8012, KLR-8016	Mono-, hydroxy- and di-carboxylic fatty acids (linear and branched)	Oxidised glycerolipids of animal and plant origin, plant waxes

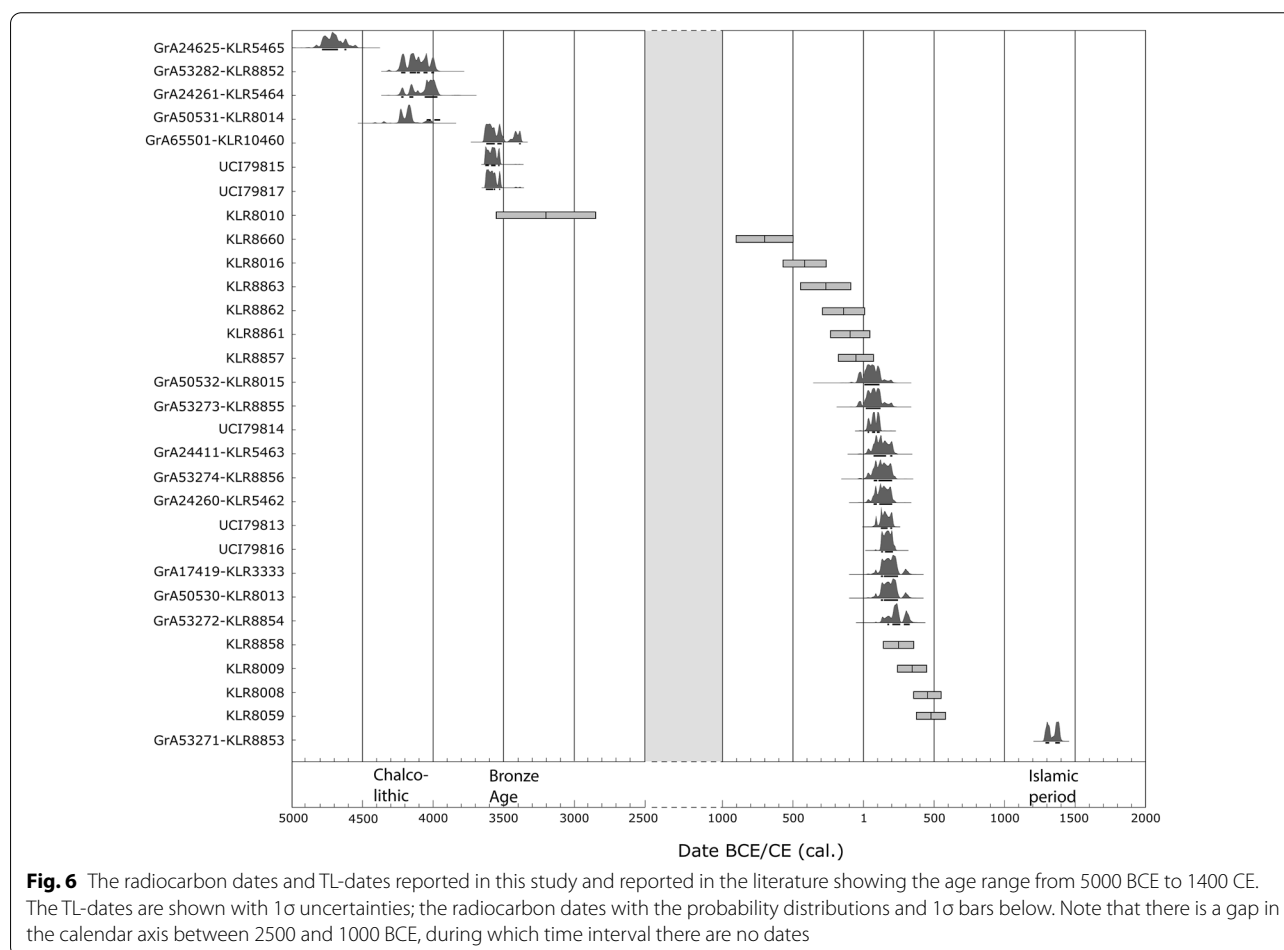


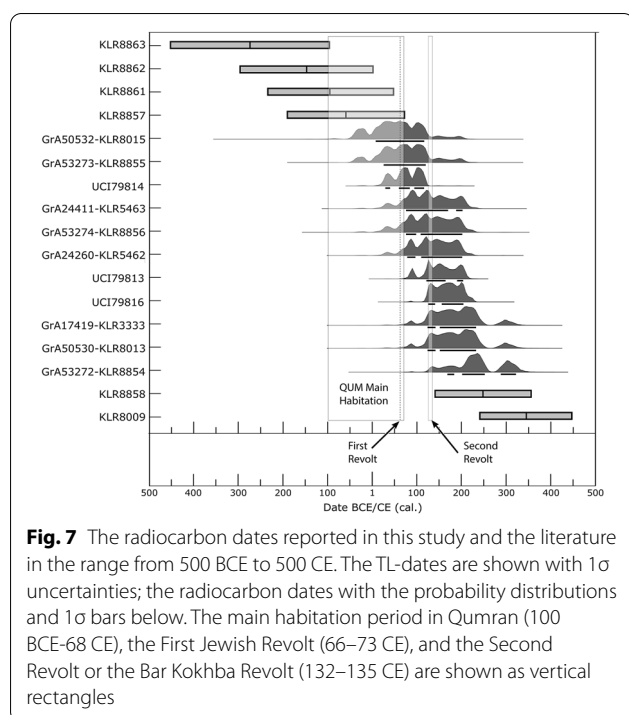
**Fig. 6** The radiocarbon dates and TL-dates reported in this study and reported in the literature showing the age range from 5000 BCE to 1400 CE. The TL-dates are shown with  $1\sigma$  uncertainties; the radiocarbon dates with the probability distributions and  $1\sigma$  bars below. Note that there is a gap in the calendar axis between 2500 and 1000 BCE, during which time interval there are no dates

but they plot in an area clearly distinct from the Qumran samples in the SPCA plot (Fig. 4). The two oldest samples KLR-8860 and KLR-8863 are the only ones placed inside the Qumran ellipsis but predate the Qumran habitation phase beginning ca. 85 BCE.

#### The organic residues

The organic residues were analysed in four ceramic samples, two sherds TL-dated to the Byzantine period, one sherd dated 568–258 BCE, and one undated sherd. The

samples contained glycerolipids as the main component, in relevant amounts. The presence in all samples of dicarboxylic acids (*e.g.*, nonanedioic acid, peak #17), of hydroxy-acids, and the co-presence of unsaturated *cis* and *trans* octadecenoic acid isomers and of 10-oxooctadecanoic acid (#49) may indicate the oxidation undergone by the material during heating (cooking) processes in presence of oxygen, but they can also result from degradation processes occurring during burial, ascribable to microbial metabolism.



The observed profiles of the above-mentioned fatty acids are non-specific, only allowing us to hypothesize the presence of plant lipids or animal fat, or a mixture of both. The presence of plant lipids is sustained by the detection in the neutral fraction of long chain alcohols and hydrocarbons (alkanes and alkenes), particularly abundant in samples KLR-8008 and present in traces in

KLR-8009 and KLR-8012: these can derive from plant epicuticular waxes extracted from vegetables [70, 71] possibly cooked in the potteries. A predominance of odd over even chain length alkanes would have further supported the occurrence of cuticular waxes, however, this was not observed in this case, leaving the discussion open for the origin of these species in the neutral fractions. Interestingly, the same sample (KLR-8008) contains a relevant amount of long chain ketones in the neutral fraction (Fig. 5b, peaks #26, 29–39 in the neutral fraction), whose presence is consistent with heating process undergone by the lipids during cooking [72, 73].

Other molecular markers mentioned in the literature for the assessment of food residue include isoprenic fatty acids, ω-(o-alkylphenyl)alkanoic acids, β-sitosterol and polyunsaturated fatty acids (PUFAs). None of these species was detected in the chromatograms. Conversely, the concomitant presence of non-negligible amounts of branched and odd-chain fatty acids (mainly C<sub>15</sub> and C<sub>17</sub>) and of cholesterol (Fig. 5d, peak #62) in samples KLR-8009 and KLR-8012 demonstrate the simultaneous presence of lipids of animal origin [74]. These odd-branched chain fatty acids are common in ruminant fats but may also have a bacterial origin [75].

Finally, the presence of a relatively high amount of contaminants such as phthalates can be ascribed to the plastic zip bags which were employed for sample shipment. Nonetheless, their presence did not affect the interpretation of the chromatographic profiles and did

**Table 9** Radiocarbon dates of materials from the Christmas Cave reported in other studies

AMS lab No	KLR lab No	Sample material	Age (BP)	δ <sup>13</sup> C (‰)	C%	Calibrated age range (1σ)	Calibrated age range (2σ)	Ref.
GrA-17427	3334	Green wool QUM543 QCC230 (Old 528)	1905 ± 30	− 20.70	44.1	CE 80–205	CE 30–220	A
GrA-24260	5462			− 20.39	44.8			
GrA-17423	3336	Red wool QUM544 QCC184 (old 530)	1915 ± 30	− 19.05	44.8	CE 75–200	CE 25–215	A
GrA-24411	5463			− 20.39	46.9			
GrA-24261	5464	Charcoal QUM545 QCC174 CC III cave 14 wood	5230 ± 45	− 21.71	69.1	BCE 4215–3975	BCE 4230–3960	A
GrA-24265	5465	Charred wood QUM546 QCC174, Tr III w end of tree amongst rock formation	5845 ± 45	− 9.22	42.0	BCE 4785–4620	BCE 4830–4550	A
GrA-17419	3333	Textile QUM527 QCC230	1850 ± 40	− 19.65	42.9	CE 130–235	CE 80–325	A
GrA-65501	10,430	Textile, linen, IAA-585785, QCC585 QCC785	4745 ± 35	− 24.32	43.1	BCE 3630–3385	3635–3380	B
UCI-79816	-	Fabric (flax)	1870 ± 15	− 24.3	n/a	CE 130–210	CE 125–220	C
UCI-79814	-	Rope (flax)	1950 ± 15	n/a	n/a	CE 30–115	CE 25–120	C
UCI-79813	-	Rope (flax, hemp)	1900 ± 15	− 25.3	n/a	CE 120–205	CE 80–210	C
UCI-79817	-	Fabric (flax, hemp)	4760 ± 15	− 24.3	n/a	BCE 3625–3530	BCE 3630–3520	C
UCI-79815	-	Fabric (flax, hemp)	4770 ± 15	n/a	n/a	BCE 3630–3530	BCE 3630–3525	C

The <sup>14</sup>C dates are recalibrated with the latest calibration curve IntCal20 [32]. See text for details. References: A: Rasmussen et al. [9]; B: Taylor et al. [88]; C: Murphy et al. [12]

not interfere with the determination of other organic molecules.

The obtained results therefore sustain the hypothesis of the occurrence of a mixture of different fats and oils, with variable degree of degradation and oxidation, deriving from the use of the vessels as cooking pots for different commodities containing plant and animal lipids.

#### Who visited the Christmas Cave and when?

The Christmas Cave is one of the major refuge caves in the northern Judean Desert. Its small, hidden entrance, the wide and comfortable inner passages, and its relatively easy access, made it a preferred temporary shelter in several periods, most notably during the times of Jewish rebellions against Roman rule in Judaea-Palaestina in the first and second centuries CE. The relatively large amount of material and ecofactual assemblages testify to its regional importance. It should be noted that no other large caves are known anywhere along the course of Naḥal Qidron, a fact that also singles out the Christmas Cave as the most important natural hideout in this drainage basin. The availability of seasonal waterholes in the valley below the cave, and the easy access granted through the chain of desert trails, also made it a favourable hideout.

The archaeological finds discovered in the Christmas Cave indicate that human activity in the cave began during the Late Chalcolithic period. The nature of these late prehistoric occurrences is unclear, also in terms of the present findings, but it has been suggested that the Judean Desert cliff caves were used as temporary refuge places at times of societal unrest [60, 64, 76]. The mineralogy of the ceramic sherd KLR-8010 is characterized by a different composition than the rest of the pottery from later periods. Its fabric has large granitic inclusions, very poorly sorted felsic minerals, calcareous rock fragments, and the presence of Ca-based silicates as shown by XRD and FTIR indicates a high and oxidizing firing temperature (Additional file 1) (also see [77] for a description of the different Chalcolithic petrographic groups). On the other hand, the chemical data highlight that this sherd presents a very distinctive geochemical signature, different from the rest of the analysed potsherds (Fig. 4).

Following a period without occupation according to the dates available, activity was next seen again in the Early Bronze Age stage IA. This is supported by three radiocarbon dates and possibly one TL-date (KLR-10430/GrA-24261, UCI-79817, UCI-79815, and KLR-8010). From an archaeological perspective, however, the Early Bronze Age IA activity seems to be an isolated phenomenon in the regional perspective.

Considering the series of radiocarbon- and TL-dates and two coins from the days of Agrippa I and Pontius

Pilate, both found during the recent survey of the cave [6], it is likely that the Christmas Cave served as a refuge cave during the First Jewish Revolt (ca. 68 CE), a time when Josephus specifically indicates that people fled from Jericho to the hills ahead of Vespasian's army (*War* 4.449–51). It seems possible also that the cave served refugees fleeing from Jerusalem and its hinterland, located less than a day's walk upstream. Several villages located on the desert margins east of Jerusalem are known to have existed till at least the First Revolt, for example Bethphage (Beit Pagge) and Bethany (Beit 'Anyā), as well as other sites in their vicinity, including Bethlehem ([78]: 96–110, 310). These villages and others are possible candidates for being the home settlements of refugees fleeing to the Christmas Cave. However, the provenances of the ceramics point to 3 to 4 groups of clay resources, where likely only one can originate from this area. The results obtained in the present study are in agreement with a larger technological and provenance study developed for Qumran and Jericho pottery [79]. This later study established that most of Qumran pottery was made of pure clay containing fragments of shales, and none of this pottery, especially the “scroll jars”, was assigned to the Wadi Qumran clay banks.

It should be remembered that ca. 4 km downstream from the Christmas Cave, north of the outlet of Naḥal Qidron Valley into the Dead Sea lay the harbour of Khirbet Mazin, established in the Hasmonean era, likely under Alexander Jannaeus (ca. 85 BCE), and occupied through the Roman period. In addition, several complexes known as “cell sites” yield evidence for activity during the early years of the First Revolt. The main cluster of remains has been found on the southern bank of the canyon at a site called “Qidron South”, where dozens of coins dated to the 2<sup>nd</sup> year of the revolt (ca. 68 CE) were found in the 1993 excavations ([80]; see also [81, 82]). Further numismatic evidence was collected from the area of the “Cave of the Coin”, ca. 2 km south of the Qidron Outlet [83]. In 68 CE Vespasian's troops conquered Jericho and the Qumran area thereafter creating a camp at Jericho and occupying the site of Qumran (the Period III occupation, see map of the Roman military movements Fig. 5.1 in [84]; see also [85]). Notwithstanding the geographic proximity, it seems possible that the Qidron Outlet cluster was operated by rebels during the early stages of the First Revolt, possibly as part of a guerrilla warfare intended to interrupt the conquest of the western shore of the Dead Sea (e.g., Ein Gedi) by Roman army units, while the Christmas Cave possibly served refugees fleeing from the Judean Highlands and elsewhere (whether this activity should be interpreted to have been limited to the early rather than the more advanced stages of the revolt is difficult to decide on the basis of the current



evidence, even if one would take into account Josephus's statement that later on all escape from Jerusalem was cut off; *War* 4.476). This is, of course, only a hypothesis which is consistent with our observations; it does require further testing.

The Bar Kokhba coin found in the British excavations, as well as the looted coins purchased by this team, and the Roman denarius from the days of Nerva found in a nearby cave in the new survey [6], all indicate that by the end of the Bar Kokhba Revolt the Christmas Cave served once again for temporary refuge. Several radiocarbon dates, on a variety of artefacts and ecofacts, indicate that during the Second Revolt the occupation of the cave was more prolonged or more frequent than during the First Revolt. To be as precise as we can, it is safe to say that the oldest half of the dates are consistent with the First Revolt at the  $2\sigma$  level; for the Second Revolt, this is the case for practically all dates, which otherwise cover the range from roughly 50 BCE to 350 CE. The origin of the refugees in this case is less clear, especially owing to the lack of archaeological data regarding the Jerusalem eastern hinterland at that time. Jerusalem itself was emptied from its Jewish population during the First Revolt. The Christmas Cave could have served refugees from Jericho, which continued to have a Jewish population, and also from Bethbassi, Herodion, and the Bethlehem region, or the Judean Highlands and wilderness, as most refuge caves opening into the main valleys draining the eastern flank of Judea towards the Dead Sea (see [6] for a detailed reconstruction).

It is unlikely that any occupants of the cave came from Qumran. Our analysis of the ceramic material exhibits 3–4 different sources of the clay. In addition, the ceramic material reflects various technological production methods. It seems that only two of the ceramic sherds could be derived from the Qumran area. These two sherds are, however, older than the main habitation period in Qumran. Three other sherds are TL-dated in accordance with the Qumran settlement, but their chemistry and mineralogy are different from ceramic materials from Qumran indicating that they do not originate from the Qumran area. The organic analyses of the sherds show traces of decayed organic material stemming from both plants and animal fat, including the effect of cooking the food stuff.

According to Allegro's testimony ([2]: 121–122), his archives and the meagre remains found in the recent survey ([6]: 47), the TL-dates and a single radiocarbon date, the Christmas Cave was also ephemerally used during the Byzantine and Islamic eras. It is possible that the single date from the Mamluk period in the present study (GrA-53271/KLR-8858) is related to Islamic-period pottery collected by Allegro's DSSF team. The phenomenon of returning to refuge cliff caves in later periods is attested

also in other instances in the Judean Desert, *e.g.*, in the Murabba'at caves located ca. 12 km south of the Christmas Cave [76, 86, 87]. The extensive use of caves, rock shelters and built structures in the Lower Naħal Qidron Area for seasonal retreats of monks during the Byzantine and Early Islamic periods [82] may also account for the scarce evidence from the Christmas Cave during these periods.

## Conclusions

New radiocarbon dates and TL-dates are presented, which collectively demonstrate intermittent occupation of the Christmas Cave for more than 6000 years. There is a concentration of evidence that coheres with the impression that this was a refuge cave of the Bar Kokhba Revolt. However, it seems there were multiple other visits to this cave.

In terms of chronology there is an overlap between the occupation of the Qumran settlement and some use of the Christmas Cave, in the first century BCE and first century CE. However, apart from a chronological correlation there is nothing in the data that indicates a closer connection between the people who used the Christmas Cave and the occupants of Qumran in the main phase of habitation. This supports the general notion of dichotomy between the phenomenon of Qumran and related caves and that of the refuge cliff caves distributed in other parts of the Judean Desert, to where rebels and refugees from Judea fled in times of stress, *i.e.*, during the First and Second Jewish Revolts. The new data presented in this study confirm that there is no material reason to connect the Christmas Cave with Qumran.

In conclusion, the new evidence presented in this study is in agreement with the textile evidence, which also indicates an origin different than Qumran. This study tentatively suggests a connection with villages from the Judean Highlands east of Jerusalem as a possible place of origin for the refugee occupants of the Christmas Cave.

Overall, in deploying multiple scientific methods we can see how it is possible to define the dating of human inhabitation of the cave with much more accuracy, thus allowing for a more varied and expansive understanding of how the cave was used in different times. While materials are likely concentrated in the mid-second century, the cave clearly attracted diverse people over the millennia. We have also been able to test how the people who came here may have related to other places occupied concurrently. Further comparative studies using such methods would undoubtedly lead to clearer specificity of such relationships and occupations.

## Abbreviations

DSSF: Dead Sea Scrolls Foundation; TL: Thermoluminescence; EBAF: École Biblique et Archéologique de Franaise; QCC: Qumran Christmas Cave (EBAF designation); V-PDB: Vienna PeeDee Belemnite; BP: Before Present, defined unit for 14C-time; EA/IRMS: Element analyzer/isotope ratio mass spectrometry; AMS: Accelerator Mass Spectrometry; AAA: Acid–Alkali–Acid; LA-ICP-MS: Laser ablation Inductively Coupled Mass Spectrometry; NdYAG laser: Neodymium-doped yttrium aluminium garnet laser; XPL: Crossed polarized light; PPL: Plane polarized light;  $\mu$ -XRF: Micro-X-ray fluorescence; FTIR: Fourier Transform Infrared spectroscopy; XRD: X-ray Diffraction; GC–MS: Gas Chromatography Mass Spectrometry; BSTFA: N,O-Bis(trimethylsilyl)trifluoroacetamide.

## Supplementary Information

The online version contains supplementary material available at <https://doi.org/10.1186/s40494-022-00652-2>.

**Additional file 1.** Pictures of selected samples. X-ray diffraction data. FT-IR spectra and second derivatives data. Petrographic data. Maximum firing temperatures determinations.

## Acknowledgements

Jan Gunneweg and Jean-Baptiste Humbert are thanked for initiating much of this work and for many years of unflinching support. Pia Klingenberg Hausmann is thanked for technical assistance.

## Authors' contributions

Conceived and designed the experiments: KLR, JvdP, GD, and JT. Performed the field work: RP, AF, and UD. Performed the chemical analyses: JvdP, KLR, TD, MPC, FM, and ID. Analyzed the data: TD, KLR, GdIF, JvdP, MPC, FM, and ID. Contributed with archaeological, archival, and regional information and perspective: RP, AF, UD, JT, OS, NS, GD, JT, and MP. Wrote the paper, with input and comments from all other participants: KLR. All authors read and approved the final manuscript.

## Funding

The present work has not been separately funded.

## Availability of data and materials

Data are available upon request from the authors.

## Declarations

### Ethics approval and consent to participate

Not applicable.

### Competing interests

The authors declare that they have no competing interests.

## Author details

<sup>1</sup>Institute of Physics, Chemistry and Pharmacy, University of Southern Denmark, Campusvej 55, 5230 Odense M, Denmark. <sup>2</sup>Center for Isotope Research, University of Groningen, Nijenborgh 46, 9747 AG Groningen, the Netherlands. <sup>3</sup>Department of Chemistry and Industrial Chemistry, University of Pisa, Via Giuseppe Moruzzi, 3, 56124 Pisa, Italy. <sup>4</sup>Laboratorio de Petrología Y Conservación Cerámica, Universidad Nacional de Catamarca-CONICET, Escuela de Arqueología Campus Universitario, Belgrano 300, 4700 Catamarca, Argentina. <sup>5</sup>Cranfield Forensic Institute, Cranfield University, Defence Academy of the United Kingdom, Shrivenham SN6 8LA, UK. <sup>6</sup>Institute of Earth Sciences, The Hebrew University of Jerusalem, 91904 Jerusalem, Israel. <sup>7</sup>Institute of Archaeology, The Hebrew University of Jerusalem, 91905 Jerusalem, Israel. <sup>8</sup>Israel Antiquities Authority, Jerusalem, Israel. <sup>9</sup>Dr. Teol, (University of Copenhagen), 1916 18th St., Apt. E206, Bellingham, WA 98225, USA. <sup>10</sup>Kings College London, 22 Kingsway, London WC2B 6NR, UK. <sup>11</sup>Qumran Institute, University of Groningen, Oude Boteringestraat 38, 9712 GK Groningen, The Netherlands.

Received: 12 October 2021 Accepted: 18 January 2022

Published online: 05 February 2022

## References

- Humbert J-B, Fidanzio F, editors. *Khirbet Qumran et 'Ain Feshkha II: Grotte 11Q*. Göttingen: Academic Press, Éditions Saint-Paul, Fribourg, Suisse/Vandenhoeck & Ruprecht, Göttingen; 2019.
- Allegro JM. *The search in the desert*. New York: Doubleday; 1964.
- Taylor JE. *Babatha's Sisters: Judean women refugees in the cave of letters and the Christmas Cave*. *Strata: Bulletin of the Anglo-Israel Archaeological Society*; 2021. (forthcoming).
- Bélis M. Des textiles, catalogues et commentaires. In: Humbert J-B, Gunneweg J, editors. *Khbirat Qumran et 'Ain Feshkha*. Göttingen: Academic Press Freiburg, Vandenhoeck & Ruprecht; 2003. p. 207–76.
- Porat R, Eshel H, Frumkin A. Remains from the days of the revolts against the romans from caves in the lower Kidron region. *Jud Samaria Res*. 2007;16:231–64.
- Porat R, Eshel H, Frumkin A. The Christmas Cave in the lower part of Nahal Kidron Refuge caves of the Bar Kokhba Revolt, Israel Exploration Society, vol. 2. Jerusalem: Israel Exploration Society; 2009. p. 31–52.
- Porat R, Davidovich U, Frumkin A, editors. *Environmental setting of the Christmas Cave, Judean Desert, Israel*. *Outdoor Qumran and the Dead Sea*. Jerusalem: COST; 2012.
- Porat R. Christmas Cave. In: Frumkin A, editor. *Atlas of the Holy Land*. Jerusalem: Magnes; 2015. p. 230–1.
- Rasmussen KL, Gunneweg J, Doudna G, Taylor J, Bélis M, van der Plicht J, et al. Cleaning and radiocarbon dating of material from Khirbet Qumran. In: Gunneweg J, Greenblatt C, Adriaens A, editors., et al., *Bio-culture and material culture at qumran—papers from a cost action G8 working group meeting held in Jerusalem, Israel on 22–23 May 2005*. Stuttgart: Fraunhofer IRB Verlag; 2006. p. 139–63.
- Shamir O. Textiles and garments from Qumran—Chalcolithic and Roman periods. In: Gunneweg J, Greenblatt C, Adriaens A, editors. *Bio- and Material cultures at Qumran*. Jerusalem: Fraunhofer IRB Verlag; 2006. p. 285–96.
- Sukenik N, Shamir O. Qumran textiles and the garments of Qumran's inhabitants. *Dead Sea Discov*. 2011;18(2):206–25.
- Murphy TM, Ben-Yehuda N, Taylor RE, Southon JR. Hemp in ancient rope and fabric from the Christmas Cave in Israel: talmudic background and DNA sequence identification. *J Archaeol Sci*. 2011;38(10):2579–88.
- Müller M, Papiz MZ, Clarke DT, Roberts MA, Murphy BM, Burghammer M. Identification of the textiles using microscopy and synchrotron radiation X-ray fibre diffraction. In: Humbert J-B, Gunneweg J, editors. *Khbirat Qumran et 'Ain Feshkha II*. Göttingen: Academic Press Fribourg, Vandenhoeck & Ruprecht; 2003. p. 277–86.
- Shamir O, Sukenik N. The Christmas Cave textiles compared to Qumran textiles. *ATN (Archaeological Textiles Newsletter)*. 2010;51:26–30.
- Yadin Y. The finds from the Bar Kokhba period in the Cave of the Letters. Jerusalem 1963.
- Sheffer A, Granger-Taylor H. Textiles from Masada—a preliminary selection. In: Aviram J, Foerster G, Netzer E, editors. *Masada IV*. Jerusalem: Israel Exp; 1994. p. 153–256.
- Shamir O. Dress, hellenistic and roman period. In: Master DM, editor. *The Oxford encyclopedia of the Bible and archaeology*. New York: Oxford University Press; 2013.
- Cleland L, Davies G, Llewellyn-jones L. *Greek and Roman Dress from A to Z*. London and New York. 2007.
- Sukenik N, Shamir O, Rottoli M, Bélis M. Textiles and Strings from Qumran Cave 11. In: Fidanzio M, Humbert J-B, editors. *Khbirat Qumran et 'Ain Feshkha IVA: Qumran Cave 11Q Archaeology and New Scroll Fragments: Novum Testamentum Et Orbis Antiquus*; 2019.
- Benoit P, Milik JT, de Vaux R. *Les Grottes de Murabba'at discoveries in the Judean desert 2*. Oxford: Clarendon Press; 1961.
- Yadin Y. Expedition D. *Israel Explor J*. 1962;12:227–57.
- Lewis N, Yadin Y, Greenfield JC. *The documents from the Bar Kokhba period in the cave of letters (Judean Desert Studies 2)*. Jerusalem: Israel Exploration Society/Hebrew University of Jerusalem/Shrine of the Book; 1989.
- Cotton HM, Yardeni A. *Discoveries in the Judean desert XXVII—Aramaic, Hebrew, and Greek documentary texts from Nahal Hever and other sites, with an appendix containing alleged Qumran Texts (The Seiyal Collection II)*. Discoveries in the Judean Desert. 1997. XXVII.
- Yadin Y, Greenfield JC, Yardeni A, Levine BA. *The Documents from the Bar Kokhba Period in the Cave of Letters, Hebrew, Aramaic and*

- Nabatean-Aramaic Papyri (Judean Desert Series 3). Jerusalem: Israel Exploration Society/Institute of Archaeology, Hebrew University/Shrine of the Book; 2002.
25. Eshel H, Zissu B. The Bar Kokhba revolt: the archaeological evidence. Jerusalem: Yad Izhak Ben Zvi; 2019.
  26. Dee MW, Palstra S, Aerts-Bijma AT, Bleeker M, De Bruijn S, Ghebru F, et al. Radiocarbon dating at Groningen: new and updated chemical pretreatment procedures. *Radiocarbon*. 2020;62(1):63–74.
  27. Aerts-Bijma AT, van der Plicht J, Meijer H. Automatic AMS sample combustion and CO<sub>2</sub> collection. *Radiocarbon*. 2001;43(2A):293–8.
  28. Van der Plicht J, Wijma S, Aerts A, Pertuisot M, Meijer H. The Groningen AMS facility: status report. *Nucl Instrum Methods B*. 2000;172:58–65.
  29. Mook WG. Introduction to isotope hydrology: stable and radioactive isotopes of hydrogen, carbon, and oxygen. London: Taylor and Francis; 2006.
  30. Mook WG, Van Der Plicht J. Reporting <sup>14</sup>C activities and concentrations. *Radiocarbon*. 1999;41(3):227–39.
  31. Ramsey CB. Bayesian analysis of radiocarbon dates. *Radiocarbon*. 2009;51(1):337–60.
  32. Reimer PJ, Austin WE, Bard E, Bayliss A, Blackwell PG, Ramsey CB, et al. The IntCal20 Northern Hemisphere radiocarbon age calibration curve (0–55 cal kBP). *Radiocarbon*. 2020;62(4):725–57.
  33. Hong D, Kim M, Choi J, El-Faramawy N, Göksu H. Equivalent dose determination of single aliquot regenerative-dose (SAR) protocol using thermoluminescence on heated quartz. *Nucl Instrum Methods Phys Res, Sect B*. 2006;243(1):174–8.
  34. Kreuzer S, Schmidt C, Fuchs MC, Dietze M, Fischer M, Fuchs M. Introducing an R package for luminescence dating analysis. *Ancient TL*. 2012;30(1):1–8.
  35. Olley J, Caitcheon G, Murray A. The distribution of apparent dose as determined by optically stimulated luminescence in small aliquots of fluvial quartz: implications for dating young sediments. *Quatern Sci Rev*. 1998;17(11):1033–40.
  36. Liritzis I, Kitis G, Galloway RB, Vafiadou A, Tsiliganis N, Polymeris G. Probing luminescence dating of archaeologically significant carved rock types. *Mediterr Archaeol Archaeom*. 2008;8(1):61–79.
  37. Grün R. The DATA program for the calculation of ESR age estimates on tooth enamel. *Quat Geochronol*. 2009;4(3):231–2.
  38. Golitko M, Terrell JE. Mapping prehistoric social fields on the Sepik coast of Papua New Guinea: ceramic compositional analysis using laser ablation-inductively coupled plasma-mass spectrometry. *J Archaeol Sci*. 2012;39(12):3568–80.
  39. Feveile C, Jensen S, Rasmussen KL. Produktion af drejet keramik i Ribeområdet i sen yngre germansk jernalder: Proveniensbestemmelse ved hjælp af magnetisk susceptibilitet og termoluminescens. *KUML*. 1998;1997:143–59.
  40. Rasmussen KL. Ny arkæometrisk metode til proveniensbestemmelse af keramik. *Arkæologiske Udgravninger i Danmark*. 1999:17–26.
  41. Rasmussen KL. Focus: provenance of ceramics revealed by magnetic susceptibility and thermoluminescence. *J Archaeol Sci*. 2001;28(5):451–6.
  42. Rasmussen KL. On the provenance and firing temperature of pottery. In: Humbert J-B, Gunneweg J, editors. *Khirbet Qumran et 'Ain Feshkha II, Novum Testamentum et Orbis Antiquus, Series Archaeologica 3*. Göttingen: Academic Press Fribourg, Vandenhoeck & Ruprecht; 2003.
  43. Rasmussen KL, Kristensen HK. Proveniensbestemmelser af brændt ler i middelalderlige bygninger. *Bygningsarkæologiske Studier*. 2001–2002. p. 83–93.
  44. Rasmussen KL, Lund J. On the clay provenance of rhodian transport amphorae. In: Eiring J, Lund J, editors. *Transport amphorae and trade in the eastern mediterranean, monographs of the Danish Institute in Athens, vol. 5*. Danish Institut i Athen; 2004. p. 325–7.
  45. Petersen K, Rasmussen KL, Rasmussen P, von Platen-Hallermund F. Main environmental changes since the Weichselian glaciation in the Danish waters between the North Sea and the Baltic Sea as reflected in the molluscan fauna. *Quatern Int*. 2005;133:33–46.
  46. Rasmussen KL, Hjeremind J. Bestemmelse af proveniens og brændingstemperatur på tidligmiddelalderlig keramik, lerklining m.v. fra Viborg og Spangsbjerg. In: Iversen M, Robinson DE, Hjeremind J, Christensen C, editors. *Viborg Sønderø 1018–1030, Arkæologi og naturvidenskab i et værkstedområde fra vikingetid*. Jysk Arkæologisk Selskabs Skrifter 52: Højbjerg; 2006. p. 423–37.
  47. Vera SD, Guillermo A, Rasmussen KL. Prácticas alfareras, tecnología y cronología durante los períodos Tardío e Inca en el sector meridional del Valle de Abacán. *Tradiciones y rupturas: el caso de Costa de Reyes N° 5* (Tinogasta, Catamarca, Argentina). *Latin Amer Antiq*. 2019;30(1):70–90.
  48. Rasmussen KL, Guillermo A, Bond AD, Mathiesen KK, Vera SD. Pottery firing temperatures: a new method for determining the firing temperature of ceramics and burnt clay. *J Archaeol Sci*. 2012;39(6):1705–16.
  49. Tite M. Determination of the firing temperature of ancient ceramics by measurement of thermal expansion: a reassessment. *Archaeometry*. 1969;11(1):131–43.
  50. Menges F. *Spectragryph*. Dr. Friedrich Menges Software-Entwicklung; 2016.
  51. De Benedetto G, Laviano R, Sabbatini L, Zamboni P. Infrared spectroscopy in the mineralogical characterization of ancient pottery. *J Cult Herit*. 2002;3(3):177–86.
  52. Akyuz S, Akyuz T, Basaran S, Bolcal C, Gulec A. Analysis of ancient potteries using FT-IR, micro-Raman and EDXRF spectrometry. *Vib Spectrosc*. 2008;48(2):276–80.
  53. Shoval S. Using FT-IR spectroscopy for study of calcareous ancient ceramics. *Opt Mater*. 2003;24(1–2):117–22.
  54. Shoval S, Paz Y. Analyzing the fired-clay ceramic of EBA Canaanite pottery using FT-IR spectroscopy and LA-ICP-MS. *Periodico di mineralogia*. 2015;84(1).
  55. Shoval S, Yadin E, Panczer G. Analysis of thermal phases in calcareous Iron Age pottery using FT-IR and Raman spectroscopy. *J Therm Anal Calorim*. 2011;104(2):515–25.
  56. Shoval S. Fourier transform infrared spectroscopy (FT-IR) in archaeological ceramic analysis. *The Oxford Handbook of Archaeological Ceramic Analysis*. 2017.
  57. Blanco-Zubiaguirre L, Ribechini E, Degano I, La Nasa J, Carrero JA, Iñáñez J, et al. GC-MS and HPLC-ESI-QToF characterization of organic lipid residues from ceramic vessels used by Basque whalers from 16th to 17th centuries. *Microchem J*. 2018;137:190–203.
  58. Cubilla-Montilla MI. *Contribuciones al análisis biplot basadas en soluciones factoriales disjuntas y en soluciones sparse*. Salamanca: Doctoral dissertation, Universidad de Salamanca; 2019.
  59. Jolliffe IT, Trendafilov NT, Uddin M. A modified principal component technique based on the LASSO. *J Comput Graph Stat*. 2003;12(3):531–47.
  60. Davidovich U. Late chalcolithic period in the Judean desert: identification, settlement pattern and material culture as a basis for social and environmental reconstruction. MA Thesis. Jerusalem: The Hebrew University of Jerusalem; 2008.
  61. Shamir O. Continuity and discontinuity in neolithic and chalcolithic linen textile production in the Southern Levant. In: Schier W, Pollock S, editors. *The competition of fibers: early textile production in Western Asia, Southeast and Central Europe (10,000–500 BC)*. Oxford and Philadelphia: Oxbow Books; 2020. p. 27–37.
  62. Yekutieli Y. Early Bronze Age IA of Southwestern Canaan. In: Wolff SR, editor. *Studies in the Archaeology of Israel and Neighboring Lands in Memory of Douglas L. Esse*. Chicago and Atlanta: The Oriental Institute of the University of Chicago and The American Schools of Oriental Research; 2001. p. 659–88.
  63. Greenberg R. *The archaeology of the bronze age levant: from urban origins to the demise of city-states, 3700–1000 B.C.* Cambridge: Cambridge University Press; 2019.
  64. Davidovich U. The chalcolithic-early bronze age transition: a view from the Judean Desert Caves, Southern Levant. *Paléorient*. 2013;39(1):125–38.
  65. Jull AJT, Donahue DJ, Carmi I, D. S. Radiocarbon dating of finds. In: Schick T, editor. *The cave of the warrior: a fourth millennium burial in the Judean Desert*. Jerusalem: Israel Antiquities Authorities, Reports 5; 1998. p. 110–2.
  66. Netzer E. *Die Paläste der Hasmonäer und Herodes des Grossen*. Mainz am Rhein: von Zabern; 1999.
  67. Bar-Adon P, Greenhut Z. Excavations in the Judean Desert. *'Atiqot: Hebrew Series/תירכנב הירדים: תוקיתנב*. 1989:1\*–8\*.
  68. Stutchbury HE, Nicholl GR. *Khirbet Mazin*. Annual of the Department of Antiquities of Jordan. 1962/3;6/7:96–103.
  69. Stager LE. Farming in the Judean desert during the Iron Age. *Bull Am Sch Orient Res*. 1976;221(1):145–58.
  70. Dunne J, Mercuri AM, Evershed RP, Bruni S, di Lernia S. Earliest direct evidence of plant processing in prehistoric Saharan pottery. *Nat Plants*. 2016;3(1):16194.

71. Whelton HL, Roffet-Salque M, Kotsakis K, Urem-Kotsou D, Evershed RP. Strong bias towards carcass product processing at Neolithic settlements in northern Greece revealed through absorbed lipid residues of archaeological pottery. *Quatern Int.* 2018;496:127–39.
72. Evershed RP, Stott AW, Raven A, Dudd SN, Charters S, Leyden A. Formation of long-chain ketones in ancient pottery vessels by pyrolysis of acyl lipids. *Tetrahedron Lett.* 1995;36(48):8875–8.
73. Colombini MP, Modugno F, Ribechini E. GC/MS in the characterization of lipids. *Organic mass spectrometry in art and archaeology.* Wiley; 2009. p. 189–213.
74. Evershed RP, Mottram HR, Dudd SN, Charters S, Stott AW, Lawrence G, et al. New criteria for the identification of animal fats preserved in archaeological pottery. *Naturwissenschaften.* 1997;84(9):402–6.
75. Suryanarayan A, Cubas M, Craig OE, Heron CP, Shinde VS, Singh RN, et al. Lipid residues in pottery from the Indus Civilisation in northwest India. *J Archaeol Sci.* 2021;125:105291.
76. Popović M. Qumran as scroll storehouse in times of crisis? a comparative perspective on Judaeen desert manuscript collections. *J Study Judaism.* 2012;43(4–5):551–94.
77. Goren Y. Shrines and ceramics in Chalcolithic Israel: the view through the petrographic microscope. *Archaeometry.* 1995;37(2):287–305.
78. Zissu B. Rural Settlement in the Judaeen Hills and Foothills from the Late Second Temple Period to the Bar Kokhba Revolt. PhD Dissertation. Ramat Gan: Bar Ilan University; 2002.
79. Michniewicz J. Qumran and Jericho pottery: a petrographic and chemical provenance study: Wydawnictwo Naukowe UAM; 2009.
80. Dahari U. Region XIV: survey and excavations of caves along the fault escarpment from Nahal Kidron to Nahal Deragot. *Atiqot.* 2002;41(2):209–19.
81. Porat R, Eshel H. Judean Desert caves in the Great Revolt. In: Bar S, editor. *In the Mountains, the Lowlands and the Plains: studies presented to Adam Zertal for the 30th year of the Land of Menashe Survey.* Jerusalem 2008. p. 323–50.
82. Davidovich U, Porat R. Hermitages along the Dead Sea Escarpment: archaeological, geographical and historical exploration. In: Peleg-Barkat O, Ashkenazi J, Leibner U, Aviam M, Talgam R, editors. *Between Sea and desert: on kings, nomads, cities and monks, essays in honor of Joseph Patrich (Land of Galilee 5).* Tzemach, Ostrakon and Kinneret Academic College: Jerusalem; 2019. p. 211–31.
83. Porat R, Eshel H, Davidovich U, Frumkin A. The caves of the coin south of Nahal Kidron. *Refuge caves of the Bar Kokhba Revolt, vol. 2.* Cham: Israel Exploration Society; 2009. p. 53–67.
84. Taylor JE. Kh. Qumran in period III. In: Katharina Galor J-B, editor. *Qumran, the site of the Dead Sea scrolls: archaeological interpretations and debates, proceedings of a conference held at Brown University, Nov. 17–19, 2002.* Leiden/Boston: Brill; 2006. p. 133–46.
85. Popović M. Roman book destruction in Qumran Cave 4 and the Roman destruction of Khirbet Qumran revisited. In: Frey J, Claußen C, Kessler N, editors. *Qumran und die Archäologie: Texte und Kontexte (Wissenschaftliche Untersuchungen zum Neuen Testament 278).* Tübingen: Mohr Siebeck; 2011. p. 239–91.
86. De Vaux R. Part I: archéologie. In: Benoit P, Milik JT, De Vaux R, editors. *Les grottes de Murabba'at.* Oxford: Clarendon Press; 1961. p. 1–63.
87. Popović M. The manuscript collections: an overview. In: Brooke G, Hempel C, editors. *T&T Clark companion to the Dead Sea scrolls.* T&T Clark London; 2019. p. 37–50.
88. Taylor JE, van der Plicht J, Rasmussen KL, Sukenik N, Shamir O, Bélis M. The Radiocarbon Dates of Samples from Qumran Cave 11Q. In: Humbert J-B, Fidanzio M, editors. *Khirbet Qumran and Ain Feshkha, IV A, Cave 11Q.* Archaeology and New Scroll Fragments. Göttingen: Vandenhoeck & Ruprecht; 2019. p. 147–57.

## Publisher's Note

Springer Nature remains neutral with regard to jurisdictional claims in published maps and institutional affiliations.

Submit your manuscript to a SpringerOpen<sup>®</sup> journal and benefit from:

- Convenient online submission
- Rigorous peer review
- Open access: articles freely available online
- High visibility within the field
- Retaining the copyright to your article

---

Submit your next manuscript at ► [springeropen.com](https://www.springeropen.com)

---